Electronic-Energy and Local Property Errors at QTAIM Critical Points while Climbing Perdew's Ladder of Density-Functional Approximations

Éric Brémond,[*,†] Vincent Tognetti,[*,‡] Henry Chermette,[¶] Juan Carlos Sancho-García,[§] Laurent Joubert,[‡] and Carlo Adamo[‖,⊥]

† *Université de Paris, ITODYS, CNRS, F-75006 Paris, France*

‡ *Normandy University, COBRA UMR 6014 & FR 3038, Université de Rouen INSA Rouen, CNRS, F-76821 Mont St Aignan, France*

¶ *Université de Lyon, Institut des Sciences Analytiques, UMR 5280, CNRS, Université Lyon 1, 5 rue de la Doua, F-69100 Villeurbanne, France.*

§ *Departamento de Química Física, Universidad de Alicante, E-03080 Alicante, Spain*

‖ *Chimie ParisTech, PSL Research University, CNRS, Institute of Chemistry for Life and Health Sciences (i-CLeHS), UMR 8060, F-75005 Paris, France*

⊥ *Institut Universitaire de France, 103 Boulevard Saint Michel, F-75005 Paris, France*

E-mail: eric.bremond@u-paris.fr; vincent.tognetti@univ-rouen.fr

Abstract

We investigate the relationships between electron-density and electronic-energy errors produced by modern exchange-correlation density-functional approximations belonging to all the rungs of Perdew's Ladder. To this aim, a panel of relevant (semi)local

properties evaluated at critical points of the electron-density field (as defined within the framework of Bader's atoms-in-molecules theory) are computed on a large selection of molecular systems involved in thermodynamic, kinetic, and noncovalent interaction chemical databases using density functionals developed in a nonempirical, minimally and highly parameterized fashion. The comparison of their density- and energy-based performances, also discussed in terms of density-driven errors, casts light on the strengths and weaknesses of the most recent and efficient density-functional approximations.

1 Introduction

How one could better assess the proper quality of a density-functional approximation (DFA)? A dilemma still persists in the field of density-functional theory (DFT).[1] It is common practice to rank a DFA according to its performance on extensive reaction energy databases.[2–4] Being indeed defined as a global property, the energy criterion is expressed as a single number associated with some chosen error metrics. Its cross comparison with a reference value deserves thus to be fast and reasonably easy to perform. In this way, reaction energy databases, sometimes augmented by energy-related properties such as structures[5–8] or electronic excitations,[9–13] just to cite some of them, represent the wide majority of reference datasets used to validate and/or develop DFAs in a semiempirical fashion.

In theory, judging the DFA reliability for energies ensures its reliability for density-based properties. The Hohenberg and Kohn theorems state indeed that the exact ground-state (GS) energy of a N-electron system is expressed as a variational energy functional of its GS electron density.[1] They establish thus a unique one-to-one correspondence between the exact GS energy and density, and guarantee obtaining an exact density under the condition of getting the exact energy.[14] Nevertheless, in practice, notably within the Kohn-Sham approach of DFT (KS-DFT),[15] energies and densities are approximated after choosing an exchange-correlation term.[16] As a result, the success of a DFA in assessing reaction energy databases, independently of their size and composition, does not necessarily parallel (vide infra) with its success in modeling density-based properties.

Assessing the density provided by DFAs has actually a long history,[17–19] and was initially closely related to quantum molecular similarity issues.[20–22] In 2017, the topic has however known a recent revitalization, fostered in particular from a work by Medvedev *et al.*[23] which initiated a still ongoing debate. Despite criticisms expressed on their computational methodology,[24–29] livened up with intense comments and answers,[30–32] they came to the conclusion, in the special case of isolated atoms, that the highly parameterization of recently developed exchange-correlation density functionals improve admittedly their accuracy versus energy

properties, but can also lead to wrong densities if an overfitting occurs. In that specific case, the overparameterization of the DFA may induce spurious oscillations that finally degrade the density evaluation.[32–34]

This discussion, later extended to more 'chemically relevant' systems through the comparison between atomization energies and electron densities of diatomic molecules,[35] confirmed the decorrelation between energy and density performances in recently developed highly parameterized DFAs. However, setting apart this family, further benchmarks still based on mono- or di-atomic systems showed that climbing Perdew's Ladder of exchange-correlation approximations[36] tends to improve the quality of the density and its successive derivatives.[28,37–39] In that sense, the trend observed for nonempirical or minimally parameterized exchange-correlation approximations parallels with the one found for energy properties,[40] and constitutes a systematic improvement while concomitantly strengthening their theoretical background.

Atoms and diatomic systems used predominantly up to now as system probes are nevertheless far to be representative of the molecular compounds found in the rich chemistry landscape. Their high similarity and homogeneity makes of course the comparison of the density and its derivatives with a reference easier, but also makes the extrapolation to real-life chemical systems not trivial. We propose here to go further by analyzing the quality of the density of larger and more diverse molecules containing up to 14 atoms and usually involved to appraise the performance of DFAs versus atomization, barrier height and weak interaction energy properties.

Interestingly, targeting larger systems requires a robust and tractable measure to assess a property defined at each space position such as the density. A first approach is to calculate on a grid a global descriptor as a cumulated density distance against a reference.[37,41] It requires the definition of density overlaps through the choice of a relevant dot product, which is clearly not unique. Such an approach is *global* in the sense that each real-space point $\mathbf{r}$ is used to compute the final and unique molecular value. Typical examples are the density overlaps

already mentioned and the comparison of molecular dipole moments[42,43] that requires the knowledge of the electron density in whole space. However, such a measure is generally not recommended since it is biased by the inert behavior of the core electrons in the vicinity of the nuclei,[39] and because it requires very large integration grids to reach the appropriate accuracy (many decimal places needed for reliable overlaps) precluding its use for larger and larger molecules.

We prefer here to focus on another analysis scale that we dub as a *local* approach. There, relevant properties are scrutinized at some specific real-space points. This is a kind of coarse-grained view of molecules: only a finite (and ideally small) number of pieces of information are used to summarize the infinite information encoded in the electron density or in related functions. In that sense, local descriptors provide a more 'chemically intuitive' picture of density errors. They are usually derived from a topological analysis of the density such as the quantum theory of atoms-in-molecules (QTAIM),[44,45] or from analysis of the kinetic energy density changes studied within the electron localization function (ELF),[46] localized orbital locator (LOL),[47] or density overlap regions indicator (DORI) frameworks.[48,49]

With the aim to evaluate the quality of the density within the bonding region of a molecule, we naturally turn to the QTAIM framework, continuing along the path paved by some of us ten years ago[50] and by other groups.[51–54] Most of these studies were however not explicitly conducted for DFT development purposes, and did not initially attempt to draw guidelines for the improvement of exchange-correlation density functionals. Within this investigation, we accordingly go further not only by measuring the performance of a broad selection of DFAs belonging to the five rungs of Perdew's Ladder, but also by comparing their accuracy in modeling energy and density properties of molecular systems. In such a way, without pretending to parallel our results with the formal knowledge of the sources of errors in DFT, we investigate correlation or decorrelation between density and energy errors within different families of DFAs developed in a nonempirical, minimally or highly parameterized fashion, thus bringing closer the pure DFT and applied QTAIM communities.

2 Local QTAIM Quantities

Developed by Bader *et al.* early in the sixties, QTAIM provides a robust and physically grounded framework[55–57] based on the topology of the electron density. In a nutshell, the regional QTAIM viewpoint divides real space into nonoverlapping atomic basins separated by interatomic surfaces, providing an exhaustive partition of the three-dimensional real space.

The local counterpart relies on the inspection of the so-called critical points (CPs), defined as points where the electron-density gradient vanishes. CPs are classified in terms of the rank (*i.e.*, number of eigenvalues) and signature (*i.e.*, difference between number of positive and negative eigenvalues) of the electron-density Hessian matrix evaluated at these points. For instance, a $(3,-1)$ CP, characterized by two negative and one positive Hessian eigenvalues, corresponds to a density minimum along the atomic interaction line and to a maximum in the perpendicular plane. At an equilibrium geometry, $(3,-1)$ CPs are called bond CPs (BCPs), their presence defining the bond between two atoms in the orthodox QTAIM interpretation.

In the same way, a ring CP (RCP) is found at the frontier between three or more atomic basins forming a ring. Such a CP is encountered here in the case of the cyclobutane molecule. It corresponds to a $(3,+1)$ CP, with two positive and one negative eigenvalues of the Hessian, and is mainly used to deal with aromaticity issues.[58] It is worth remarking that two other kinds of CP exist within QTAIM, *i.e.*, $(3,+3)$ cage and (non)-nuclear attractor $(3,-3)$ CPs. They are however not deeply inspected into the present investigation.

Plethora of studies showed that BCP properties are highly correlated to bond energies in both covalent and noncovalent cases.[59–64] Among the most common and relevant features, we find the BCP location ($\mathbf{r}_{\mathrm{CP}}$), its electron-density value (ρ), and its density Laplacian value ($\nabla^2\rho$), the latter measuring the charge accumulation or depletion. All of these properties can be used to assess the quality of the density produced by a given DFA and unravel how this quality is related to a correct description of the bond. These three local descriptors will be supplemented with the electronic part (Φ_e in atomic units) of the molecular electrostatic

potential evaluated at the considered CP according to

$$\Phi_e(\mathbf{r}_{\mathrm{CP}}) = -\int \frac{\rho(\mathbf{r})}{|\mathbf{r}_{\mathrm{CP}} - \mathbf{r}|}\mathrm{d}\mathbf{r}. \tag{1}$$

With respect to the other local quantities, it provides additional information dealing with the interaction of the whole electron density of the system with the one evaluated locally at CP. Owing to its *semilocal* character, it allows to get a complementary picture of the quality of the density at CP.

Obviously, other local descriptors might have been included, such as variation rates[65,66] or some energy components, for instance the two flavors (Lagrangian and Hamiltonian) of the kinetic energy densities at CPs, or the virial field value,[67] which are often discussed in the QTAIM literature. However, their evaluation generally requires not only the electron density, but also the first-order reduced density matrices (1-RDMs). In the current practice of QTAIM processed from DFT calculations, 1-RDMs are computed using the fictitious KS system.[68] While the KS and exact densities are by definition equal (provided that the exact exchange-correlation density functional is used), the exact KS 1-RDM differs generally from the 1-RDM extracted from the exact wavefunction. As a result, such a local DFT quantity cannot be safely compared to post-Hartree-Fock references. Accordingly, only descriptors explicitly and exclusively expressed from the electron density or/and its derivatives are retained.

3 Theoretical Methods

It is common practice to rank DFAs according to their level of nonlocality within Perdew's Ladder.[36] While climbing it, the first three rungs are dedicated to (semi)local, also dubbed non-hybrid, exchange-correlation approximations. They explicitly depend on semilocal ingredients such as the density, its gradient and its Laplacian, and correspond to the local density, generalized gradient, and meta-generalized gradient approximations (LDA, GGA, and meta-GGA, respectively).

Within the DFA landscape, the enhancement factor of non-hybrids is either developed in a nonempirical fashion by identifying its constants to limit physical constraints, or by empirically optimizing its parameters taking as a reference chemical reaction databases. Table 1 reports some examples of non-hybrids. For instance, PBE is considered as nonempirical whereas BLYP is viewed like a minimally parameterized approach (*i.e.*, few parameters entering into its expression), while other cases like Minnesota density functionals, are considered as highly parameterized, their number of empirical parameters being considerably large.

The nonlocality of non-hybrids can be extended by adding a dependence into nonlocal exact-like exchange (EXX). The resulting hybrid DFA corresponds to the rung 4 of Perdew's Ladder. The development of this approximation has largely contributed to the still alive wide enthusiasm of the chemistry community for KS-DFT,[69,70] particularly with the development of the B3LYP or PBE0 models. In its global-hybrid (GH) formulation, the exchange-correlation energy is expressed such as

$$E_{xc}^{\mathrm{GH}}[\rho,\{\phi_i\}] = a_x E_x^{\mathrm{EXX}}[\{\phi_i\}] + (1-a_x)E_x[\rho] + E_c[\rho], \tag{2}$$

where E_x and E_c stands for the (semi)local exchange and correlation energy contributions, respectively, and a_x denotes the fraction of EXX energy (E_x^{EXX}) which depends on the set of occupied orbitals $\{\phi_i\}$. The transformation of GH into its range-separated exchange hybrid (RSX-H) variant further improves the estimation of such a property by splitting the Coulomb operator into a short- and long-range terms (SR and LR, respectively) such as[71–73]

$$\frac{1}{r_{12}} = \underbrace{\frac{1-[\alpha+\beta\,\mathrm{erf}(\mu r_{12})]}{r_{12}}}_{\mathrm{SR}} + \underbrace{\frac{\alpha+\beta\,\mathrm{erf}(\mu r_{12})}{r_{12}}}_{\mathrm{LR}}, \tag{3}$$

where α and $\alpha+\beta$ govern the fraction of EXX in the SR and LR terms, respectively, and μ the range-separation parameter.

Reaching the rung number 5 of Perdew's Ladder increases again the nonlocality of the approximation. It is done by adding a dependence into nonlocal correlation. A robust and now casual way to reach it is depicted by the double-hybrid (DH) model[74–76]

$$E_{xc}^{\mathrm{DH}}[\rho,\{\phi_i\},\{\phi_a\}] = a_x E_x^{\mathrm{EXX}}[\{\phi_i\}] + (1-a_x)E_x[\rho] + a_c E_c^{\mathrm{PT2}}[\{\phi_i\},\{\phi_a\}] + (1-a_c)E_c[\rho] \quad (4)$$

where a_c denotes the fraction of second-order perturbation theory (PT2) correlation energy (E_c^{PT2}) which depends on the set of occupied and virtual orbitals $\{\phi_i\}$ and $\{\phi_a\}$, respectively. By introducing nonlocal exchange and correlation, DHs (partly) correct non-hybrids regarding the one-electron self-interaction error (SIE) and its extension to many-electron systems,[77,78] but allow also the recovery of the binding nature of weak interactions. The computational effort requested to perfom a DH energy single point computation remains one magnitude larger than for GHs ($O(n^5)$ *versus* $O(n^4)$, respectively, n referring to the size of the basis set). It is nowadays common usage to alleviate it by turning on the Resolution-of-the-Identity approximation.

Like non-hybrids, GH and DH approximations can be developed in a nonempirical fashion. In that case, their expressions derive directly from the adiabatic connection formula[79] and their parameters are identified to fulfill some constraints and known conditions. In their global formulations, PBE0 and PBE-QIDH are two representative DFAs of this family (Table 1). GHs and DHs can be also developed by empirically optimizing their fractions of EXX and PT2 correlation versus reference energy databases. Within empirical variants, Table 1 reports for instance hybrids such as B3LYP and ωB97X-D, and double hybrids such as B2-PLYP and ωB97X-2. We consider here B3LYP and B2-PLYP as minimally parameterized since they introduce two or three more empirical parameters with respect to BLYP. However, we class ωB97X-D and ωB97X-2 as highly parameterized DFAs since their parameterization process involves not only the fraction of nonlocal ingredients, but also the enhancement factors of the (semi)local energy terms, increasing thus the total number of

empirical parameters to more than 30.

4 Computational Details

Except when mentioned, electronic structure and wavefunction-based computations are performed with the release C.01 of the Gaussian'16 program[80] using, for each single-point energy computation, a tight self-consistent field (SCF) convergence criteria and an ultrafine integration grid. All properties are uniformly computed with the very large def2-QZVP Ahlrichs' quadruple-ζ basis set[81] that ensures a nearly complete basis set convergence for energies but specially for densities. ωB97X-2 electronic structure computations are performed with the release 5.0.0 of the Orca program[82] at the same level of theory using a tight SCF convergence criteria, and taking advantage of the "chain-of-spheres" algorithm (COSX) variant of the 'Resolution-of-the-Identity' (RI) approximation[83] in association with the DefGrid3 integration grid.

For this benchmark investigation, we select a broad panel of 29 density functionals belonging to the five rungs of Perdew's Ladder (Table 1). We especially choose them to probe the quality of the density produced by (*i*) non-hybrid, hybrid and double-hybrid, and (*ii*) nonempirical, minimally and highly parameterized DFAs. As recommended in previous investigations dealing with the topic,[23–32] we take high-quality densities derived from the coupled-cluster singles and doubles method (CCSD) as reference.

Except for double-hybrid and post-Hartree-Fock computations, densities are produced in a self-consistent fashion by solving the KS or Hartree-Fock (HF) equations. In the specific case of double-hybrid density functionals and CCSD, SCF densities are relaxed *a posteriori* via the Z-vector technique in order to take into account the response of the molecular orbitals to the external perturbation.[84,85]

The four sets of density-corrected DFT (DC-DFT) computations[86–88] are performed by using the SOGGA11, PBE0, M06-2X and HF KS orbitals, respectively. In each set, KS

orbitals self-consistently obtained are used to compute the KS kinetic energy, and the EXX and PT2 contributions to the electron repulsion energy, while the SCF density is employed to evaluate the nuclei-electrons interaction energy, the Hartree bielectronic repulsion energy, as well as the LDA, GGA and metaGGA contributions to exchange-correlation.

For each computational approach, the evaluation of the electron density on a grid is obtained with the release 2.1.1 of the HORTON package[89] using an 'ultrafine' Becke-Lebedev molecular integration grid.[90] Section S3 in Supporting Information reports the detailed formula of the cosine, Tanimoto and Dice overlaps used in this investigation.

All QTAIM computations are performed with the AIMAll package in its version 19.02.13[91] using a 'superfine' integration grid and a Leb32 quadrature.

5 Results and Discussion

As stressed in the introduction, the most natural approach to benchmark the quality of the electron density produced by a DFA is the evaluation of the density overlap (following the Cosine, Tanimoto or Dice formula) between the probe and a reference, each density being evaluated on a very large integration grid. However, as illustrated by the mean absolute deviations reported in Tables S1 to S6 in Supporting Information, the computed overlaps for a total of 211 molecules are in most cases higher than 0.9990. The discrepancies between the different DFAs are thus encoded in the fourth decimal places. Despite the strict relationship that exists between the whole electron density and DFT energy, the numerical accuracy of this global approach is from our point of view difficult to properly assess.

As a more numerically stable alternative, we prefer here to turn on the analysis of the quality of the density at well-defined 'chemically' relevant space points of a molecular system such as the critical points derived from the QTAIM framework. Computing density errors at critical points does not provide a strict and formal correlation between electron density and energy errors. However, it depicts the quality of the density produced by a given DFA

within a 'chemically' relevant region of a molecule and allows to correlate it with an energy property governed by a molecular reactivity occurring in the same region. On this line, Grimme[92] and Cioslowski[93] already showed that local QTAIM properties are instrumental in predicting atomization energies and enthalpies of formation. Here, we will follow this path in comparing density errors at critical points with (*i*) atomization energy, (*ii*) barrier height energy, and (*iii*) weak-interaction energy errors.

To further validate our protocol of comparison between density and energy, Figure S1 in Supporting Information correlates the global electron density overlaps evaluated on an integration grid with local density errors calculated at critical points. First, it shows that the latter errors are one or two orders of magnitude larger than the former, assuring thus a more numerically stable analysis of the DFA performance. Then, it demonstrates, with one exception over 30 computational methods, that the density overlap integrated on a grid decreases linearly when the local density error at critical point increases. It thus emphasizes that for most of computational approaches, the local density error at critical point is representative of the electron density quality of the whole molecular system.

Our density versus energy benchmark starts now with the selection of 'chemically relevant' systems. To make the comparison between both properties easier, we first select three small representative benchmark sets whose two of them are designed to provide a statistical estimate of the DFA performance from extensive datasets at a considerably reduced computational cost. We especially focus on the AE6 and BH6 sets,[2,94] each of them containing six representative reactions and probing for atomization and kinetic properties, respectively. For instance, the DFA errors calculated on AE6 deviate in average only by 1.9% from the DFA errors computed on the larger reference set of 109 atomization energies from which it was generated.[2]

We complement them with six noncovalent interactions gathered in the so-called WI6 dataset. It is composed by the methane and water dimers at three different distances: the CCSD equilibrium one and two non-equilibrium ones, the first corresponding to a more

compressed system (90% with respect to the global energy minimum) and the second to a decompressed complex (by 150%). The two considered systems are actually part of the S22×5[95] and S66×8[96,97] datasets, respectively, the former being mainly maintained by London dispersion and the latter by electrostatic interactions. The whole energy benchmark set thus contains a total of 18 reference energies characterizing 18 molecular reactions ruled by short- (AE6), middle- (BH6) and long-range (WI6) bonding interactions.

The 18 molecular reactions described above involve a total of 15 main molecular structures whose QTAIM topologies computed at the reference CCSD level are depicted in Figure 1. More precisely, the AE6 dataset contains six minimum energy structures that gather a total of 29 BCPs and one RCP. The BH6 set is composed by three transition state (TS) structures which are characterized by 11 BCPs. Finally, the WI6 dataset contains six dimer (non)equilibrium structures, each of them characterized by a unique 'weak' BCP located in between both monomers as a consequence of the Poincaré-Hopf relationship.[98] The whole density benchmark set is thus composed by a total of 47 characteristic CPs in which (semi)local density-based quantities are estimated.

As already mentioned in the computational details Section, local QTAIM properties for DFAs are evaluated at the geometries optimized at a reference level in order to disentangle electronic and structural effects. While density, density Laplacian and electrostatic potential values are different for each method, this is no longer the case for the BCP location in symmetric systems. For instance, the BCP of the disulfur molecule is found exactly in the middle of the bond for all tested levels of theory. Conversely, in case of polar bonds, the BCP position is strongly related to the electronegativity differences between the two bonded atoms,[99,100] and thus constitutes a descriptor suited to assess the quality of the ionic character of a bond by the considered DFAs.

A first comparison between energy and density-based properties is depicted in Figure 2. We especially focus here on a short selection of methods belonging to the generalized gradient approximation (GGA), and to the hybrid (in the global or range-separated exchange expres-

sions) and double hybrid classes of approximation in order to measure both the influence of their rung (ruled by Perdew's Ladder) and level of parameterization on their performance. This selection is composed by three DFA families developed (*i*) in a nonempirical fashion, *i.e.* PBE, PBE0 and PBE-QIDH, (*ii*) by introducing few empirical parameters, *i.e.* BLYP, B3LYP and B2-PLYP, and (*iii*) by following an extensive empirical parameterization approach, *i.e.* B97-2, ωB97, ωB97X, ωB97X-D and ωB97X-2.

Independently of the parameterization level and interaction type, it is worth recalling that climbing Perdew's Ladder systematically improves the DFA performance with respect to energy properties.[40] For instance, going from PBE to PBE-QIDH decreases the mean absolute deviation (MAD) versus atomization energy properties (AE6 dataset) from 14.7 to 4.3 kcal mol^{-1} and from 9.5 to 0.8 kcal mol^{-1} for energy barrier heights (BH6). This large improvement corresponds to a MAD decrease of about $\sim$10 kcal mol^{-1}. The same trend is observed for the BLYP family and for the highly parameterized DFAs with a MAD decrease of about $\sim$4 and 1 kcal mol^{-1}, respectively.

The smaller amplitude decreases observed for the latter families comes from the better performance of their semilocal and global-hybrid approximation, probably induced by their empirical parameterization derived from these type of properties (*i.e.*, 6.8 and 3.8 kcal mol^{-1} for BLYP and B97-2 on the AE6 subset), with the double-hybrid approximation providing merely close MADs. Out of thermochemistry and kinetic properties, the same trend is observed for weak interactions except that the magnitude of improvement is reduced consequently due to the smaller strength of the interaction.

The role of the empirical parameterization on the energy performance is a point already taken up by previous investigations.[101,102] However, it is also important to remind that highly parameterized DFAs perform generally better than minimally or nonempirical ones within their application domain. On the other hand, nonempirical approaches have the advantage to keep less marked statistical fluctuations independently of the system size and beyond training sets.

For density-based properties calculated at CPs (Figure 2), a similar trend is observed for nonempirical and minimally parameterized density functionals. The density error for the AE6 testset is indeed reduced from 0.005 to 0.001 a.u. when going from PBE to PBE-QIDH, and from 0.003 to 0.001 a.u. for BLYP and B2-PLYP, respectively. The other local and semilocal quantities like the CP location, Laplacian of the density and electron electrostatic potential display the same decreasing trend. Still within the same dataset, going from the semilocal approximation to the double-hybrid one decreases the MAD related to these criteria of 0.008, 0.068 and 0.023 a.u, respectively, for the PBE-based family, and of 0.009, 0.045 and 0.025 a.u., respectively, for the BLYP-based one. Among this set of density functionals, PBE-QIDH is the one producing the best estimates over the whole set of density-based quantities on the AE6 testset. It is worth noticing that such local and semilocal CP quantities allow magnifying the discrepancies between the generated electron densities. For instance, for the S_2 molecule, the $(3, -1)$ density value equals 0.1969 a.u. with SVWN5 and 0.2015 a.u. at the CCSD level, while the cosine, Tanimoto and Dice overlaps between SVWN5 and CCSD densities are equal to 0.99998, 0.99993 and 0.99997, respectively.

If nonempirical and minimally parameterized DFAs improve systematically and concomitantly their performance versus energy and density-based properties while climbing Perdew's Ladder, highly parameterized methods belonging to the B97 family do not behave similarly. Among them, the B97-2 global hybrid is indeed the best performer on the AE6 testset, while it is the worst for energy properties. The addition of further empirical parameters in the more sophisticated ωB97, ωB97X, ωB97X-D and ωB97X-2 approaches is definitively not a guarantee to get an improvement of density-based performances, since the density MAD equals 0.0016 a.u. for B97-2 (GGA) and 0.0028 a.u. for ωB97X (range-separated hybrid). Their parameterization process was indeed designed to minimize their error versus extensive energy database, however for the sake of computational time saving and affordability, each single point energy was not computed in a self-consistent fashion, but from a selected guess of KS orbitals (see the corresponding references reported in Table 1). This lack of self-

consistency is probably the reason for not having a systematic improvement of density-based properties while climbing Perdew's Ladder.

As depicted in Figure 2, the performance trend obtained on the AE6 testset is also verified for molecular systems involving longer range interactions such as noncovalent ones (WI6 testset) or lengthened (forming or breaking) bonds (BH6 testset). For nonempirical and minimally parameterized methods, density errors estimated at the $(3,-1)$ CPs of TS or inter-monomer structures tend to decrease when the level of approximation increases. For instance, the density MAD values for the BH6 dataset equal 0.0035 a.u. (PBE), 0.0021 a.u. (PBE0), 0.0008 a.u. (PBE-QIDH), while highly parameterized approaches do not follow this trend. For the same dataset, the density MAD stagnates when going from ωB97X (0.0017 a.u.) to the much more time-consuming ωB97X-2 double-hybrid functional (0.0017 a.u.).

The case of ωB97X-D is particularly interesting for the WI6 testset. Indeed, the addition of a Grimme's dispersion term to the density functional divides by a factor four the energy error with respect to ωB97X-noD (0.1 versus 0.4 kcal mol^{-1}, respectively, see Table S9 within Supporting Information), a considerable breakthrough. This atom pairwise correction, which has not to be confused with self-consistent van der Waals density functionals,[103] is added on top of the KS-DFT SCF energy in order to recover the missing asymptotic correlation energy.[104] Except for some formulations that introduce a density dependency and can be turned into a self-consistent variant,[105–108] these classical potentials impact only the total energy of the system (and the shape of potential energy surfaces). This implies that in principle they should have exactly no effect on density properties, decorrelating density and energy performances, and should be therefore inadequate to partly correct the density of the uncorrected DFA.

Noticeably, for the BH6 set, the MAD for the $(3,-1)$ CPs density values is found higher with ωB97X-D (0.0021 a.u.) than for ωB97X (0.0017 a.u.), and the same observation holds for Laplacian values (0.0286 with D-correction vs. 0.0237), and also for the AE6 set. Counterintuitively, the dispersion correction deteriorates density properties for strong bonds, while

almost insensitive to noncovalent ones. This is actually due to the fact that the parameters entering the ωB97X and ωB97X-D expressions take slightly different values because they were refitted in the latter one to minimize energy errors in presence of the dispersion term.

On the contrary, by adding a nonlocal correlation contribution, the double-hybrid approximation is considered as a first-principle alternative to correct DFAs for dispersion issues. By construction, it allows correcting for both the energy and density. Taking PBE-QIDH as example, Figure 3 illustrates the impact of the nonlocal correlation term on the electron-density value at the inter-monomer $(3, -1)$ CPs for water and methane dimers by comparing the PBE-QIDH density with those produced by PBE and PBE0. As depicted above, the GGA provides the worst estimates of the density characterizing the hydrogen bond in the water dimer and the noncovalent interaction in the methane one. More precisely, it tends to overestimate the density on both examples with an error amplitude few times larger for the water (0.0013 a.u.) than for methane (0.0002 a.u.) dimer at the equilibrium distance, the error decreasing with an inter-monomer distance increase.

The addition of a 25% of EXX leading to PBE0 improves the results by decreasing the density overestimation. Increasing again the fraction of EXX to 69% by the SCF part, *i.e.*, before adding the PT2 correction (the PBE-QIDH(SCF) model), slightly underestimates the density in the weakly interacting regions. However, relaxing the density with the PT2 term (PBE-QIDH) turns the double hybrid approximation into the best method to estimate the density in this region with a density error of about 0.0002 a.u. and lower than 10^{-4} a.u., respectively. This shows that the density accuracy strongly depends on the balance between the fraction of EXX and PT2 correlation within the double-hybrid scheme.

To further confirm the performance trend obtained with the three small representative datasets, and improve the robustness of this density versus energy benchmark investigation, we complement it by assessing the QTAIM topology of 138 (out of 148) molecules gathered into the G2 atomization energy database,[109–111] 12 TS structures belonging to the DBH24 barrier height energy dataset,[112] and 27 (out of 31) dimers in weak interactions derived from

the NCB31 noncovalent bond set.[113] A detailed list of the systems involved here is reported in Section S1 in Supporting Information. We insist however on the difficulty we faced to compute the CCSD reference densities for these 177 extra molecular systems. The very large computational effort requested for some of the largest targeted molecules, notably the huge integral storage demand, forced us to leave them out of this investigation. The resulting 177 additional topologies count for a total of 727 $(3,-1)$ and 19 $(3,+1)$ additional CPs (see for instance Tables S13 to S205 within Supporting Information), all of them calculated on reference geometries provided by each dataset.

Figures S2 and S3 report the accuracy of the BLYP, PBE and B97 families of DFAs in computing the density and density-related descriptors at these CPs, and compare them with their energy performance on each dataset. As observed on the small representative datasets, a large and concomitant density and energy performance improvement is found while climbing Perdew's Ladder for the nonempirical and minimally parameterized family of DFAs. For instance, the density error on the G2 dataset goes from 0.0040 to 0.0014 a.u. for PBE and PBE-QIDH, respectively, and from 0.0024 to 0.0016 a.u., for BLYP and B2-PLYP, respectively (Figure S2). On the same set, the energy performance trend parallels and goes from 16.2 (6.8) to 4.5 (1.9) kcal mol^{-1} for PBE (BLYP) and PBE-QIDH (B2-PLYP), respectively. The same trend is observed for the DBH24 and NCB31 databases. It is also worth noticing that Figure S2 further confirms the energy and density performance stagnation of the B97 family of highly parameterized DFAs while going from the non-hybrid to the double-hybrid approximation. It results that the trends obtained on the small representative datasets compare with the ones derived from the largest ones. Moreover, in discriminating the density-based properties computed at the $(3,-1)$ and $(3,+1)$ CPs, Figures S6 and S7 show that the performance trends are independent on the type of CPs. Despite the more stable character of BCPs, a linear relationship between density errors at BCPs and RCPs can be evidenced. It thus confirms that the same conclusions can be drawn independently on the position and type of the local density descriptor.

The conclusions drawn up to now from a short DFA selection emphasize that the level of empirical parameterization decorrelates the performances for energy and density properties. It indeed tends to improve the DFA accuracy for all of the energy properties investigated here but does not improve with the same gain the density at covalent and noncovalent bonds. To confirm this trend, we extend our investigation to 20 extra highly parameterized DFAs belonging to the semilocal or hybrid classes (see Section S2 within Supporting Information). Figure 4 compares their energy and density performances on the AE6, G2, BH6, DBH24, WI6 and NCB31 datasets to those of the nonempirical PBE0 global hybrid, and classify them according to their electron density accuracy. Figures S4 and S5 in Supporting Information provide a comprehensive database by database comparison of the deviations reported in Figure 4.

At first glance, it is worth noting that the density performance of the nonempirical PBE0 cumulated over the three datasets ranks it in position 7 over 21, while a ranking over energy criteria would push it in the 19th position, far from some popular empirical DFAs. This proves again that a highly empirical parameterization does not *a fortiori* improve the quality of the density while it is supposed to do it by construction for energy. This rule of thumb is also corroborated by the R^2 coefficient of determination assessing the quality of the linear relationship between energy and density MADs (Figure 5). On each separated dataset, R^2 is lower than 0.23 (AE6 + G2 and WI6 + NCB31) and is about 0.01 for BH6 + DBH24. Over the six datasets, R^2 remains very low (0.38), showing once more the full lack of correlation between energy and density performances for highly parameterized approximations in comparison to nonempirical and minimally parameterized ones (0.83). Note that the same trends are obtained while considering separately each dataset, and that the AE6 and BH6 representative datasets provide close statistics to their larger G2 and DBH24 extensions (see Figure S4 and S5 within Supporting Information).

The top two of the best highly parameterized methods is composed by two Minnesota DFAs whose cumulated MAD is lower than 0.0086 a.u. (Figure 4). In increasing density

error order, these are the M06-2X and SOGGA11-X global hybrid approaches. Among them, M06-2X, which is 13 years old and hence among the oldest approaches benchmarked here, provides indeed very low density deviations of about 0.0021, 0.0013 and 0.0004 a.u. on the G2, DBH24 and NCB31 databases, respectively (Figure S4 within Supporting Information). It provides also the first best cumulated energy MAD (6.8 kcal mol^{-1}). They are followed by three members of the ωB97 family which are characterized by a cumulated MAD of about $\sim$0.0095 a.u. and $\sim$9.1 kcal mol^{-1} for density and energy errors, respectively. M11, MN15, N12-SX and N12 provide close cumulated density errors to PBE0. N12 is however the worst performer regarding energy errors (28.2 kcal mol^{-1}).

The remaining DFAs ranked from M05-2X to M06-HF poorly perform with a cumulative density error higher than 0.0176 a.u. which corresponds to a MAD more than twice larger than for M06-2X (Figure 4). It corresponds to density deviations of about 0.0051, 0.0042 and 0.0005 a.u. on the G2, DBH24 and NCB31 databases, respectively (Figure S4 within Supporting Information). The cumulated density error of M06-HF is the worst found in this investigation (0.0393 a.u.) however its cumulated energy error remains in the upper scale (15.6 kcal mol^{-1}), showing again the lack of correlation between energy and density performance for highly parameterized DFAs.

The most intriguing case remains nevertheless M11-L that is ranked as second to last. Despite its 19 empirical parameters, both its energy and density performances remain among the poorest of our selection. More precisely, a careful analysis of the QTAIM topology of the propyne molecule computed from its density shows a wrong description of the alkyne triple bond (Figure 6). The latter is indeed described by two $(3,-1)$ CPs located around a non-nuclear attractor. This feature, usually found in lithium clusters and caused by the very sparse charge density distributions in between the nuclei,[114–117] shows that M11-L does not satisfactorily describe the density along the triple bond.

In conclusion, the analysis of Figure 4 shows that highly parameterized density functionals provide in their large majority excellent performance versus energy properties, however their

excellent energy accuracy seems to not correlate with a good accuracy in predicting density properties, and independently of the CP type considered (see Figures S8 and S9 within Supporting Information). Among the 20 analyzed density functionals, M06-2X is the one providing the best compromise between energy and density accuracy (0.0086 a.u. and 6.8 kcal mol^{-1}, respectively). Its cumulated performance has to be compared with the ones of the B2-PLYP minimally parameterized (*i.e.*, 0.0050 a.u. and 8.6 kcal mol^{-1}) and PBE-QIDH nonempirical (*i.e.*, 0.0052 a.u. and 11.5 kcal mol^{-1}) double hybrids.

The quality of the density is finally evaluated here by measuring its impact on the density-driven error property measured over the AE6, BH6 and WI6 datasets. This concept is part of the DC-DFT approach pioneered by the Burke's group,[86–88] which decomposes DFA errors into contributions driven by the energy functional and those due to errors in the self-consistent density. Figure 7 collects the diagrams correlating the energy errors computed in a self-consistent fashion and estimated from the SOGGA11, PBE0, M06-2X and HF densities, for the previous selection of 20 highly parameterized functionals. These choices for guess densities are motivated by the following facts: (*i*) SOGGA11 is a pure (without EXX and PT2) density functional and was found as the one providing a good estimate of the density; (*ii*) PBE0 is a global hybrid including a small fraction of EXX (25%) and is considered as the nonempirical standard of this investigation; (*iii*) M06-2X includes approximatively twice the fraction of EXX (54%) and is the second best approach of this investigation; (*iv*) finally HF is underlined by several investigations to provide a self-interaction-free density that can alleviate severe DFA deficiencies.[29]

One could also wonder whether the same protocol could be applied using the CCSD electron density and CCSD natural orbitals (NOs, which diagonalize the Z-vector relaxed 1-RDM). However, this would lead to double counting of the correlation kinetic energy since the kinetic energy calculated from NOs would incorporate correlation effects to the kinetic energy that are in principle included in the exchange-correlation functional. For such reasons, post-HF methods are preferred to be not used in this density-corrected approach.

As a first observation, it is important to note that rare are the density functionals for which using a non-self-consistent density improves their accuracy in predicting energy properties (these few cases can be graphically identified by looking at points above the first bisector in Figure 7). It thus emphasizes that, when developed, highly parameterized DFAs should be parameterized in a self-consistent fashion. Moreover, we observe that plugging the density derived from a non-hybrid approximation (SOGGA11) into various exchange-correlation expressions provides very large deviations, or in other words, largely worsens the energy performances (Figure 7). Except for WI6, using the HF density provides similar deviations. The best energy agreement between non-self-consistent and self-consistent densities is obtained with the PBE0 or M06-2X global hybrid densities.

Even if we do not intend to systematically analyze the influence of the EXX fraction, such observations suggest that by reducing the one- and many-electron self-interaction errors (SIEs),[77,78] global hybrids including between 25 and ∼50% of EXX produce the best density compromise minimizing the density-driven energy error. In such a way, our findings corroborate with the ones published very recently by Santra and Martin on the extended GMTKN55 dataset.[118] They recall also that by exclusively using the PBE0 density (25% of EXX), the xDH-PBE0 doubly hybrid,[119,120] a non-self-consistent double hybrid from the xDH family,[121] succeeds to display impressive performance for an extended panel of energy and energy-related properties.[122,123] Our findings demonstrate also that, excluding WI6, the lack of correlation in the HF SIE-free density increases the density-driven error. Above all, it proves that for highly parameterized exchange-correlation expressions, the use of an accurate density does not certify to get a good estimate of the energy.

6 Conclusion

In this benchmark investigation, we concentrated on the quality of the electron density produced by a wide selection of 29 exchange-correlation density functionals belonging to

each rung of Perdew's Ladder. With respect to previous investigations that mainly evaluated density errors with respect to atomic benchmark sets, we focused on 'chemically relevant' molecular systems. Furthermore, the electron density in molecules is known difficult to analyze as a whole, particularly due to the large density amplitudes in the close neighborhood of the nuclei. We alleviated this difficulty by restricting our investigation to the study of the 'chemically relevant' bonding regions by means of local and semilocal density-dependent QTAIM quantities evaluated at the bond and ring critical points.

As a first conclusion, we evidenced that the systematic energy error improvement usually observed while climbing Perdew's Ladder is not *a fortiori* reproduced for the density criteria. More precisely, a clear dichotomy was unraveled. On the one hand, we showed that increasing the sophistication level of the exchange-correlation approximation improves concomitantly and in a remarkable way the performance of nonempirical and minimally parameterized density functionals, while, on the other hand, this was not the case for modern highly parameterized approaches. We conjectured that this disparity comes from the parameterization process, and particularly from the fact that it was not systematically carried out in a self-consistent fashion.

Then, we demonstrated that for nonempirical and minimally parameterized density functionals, the double-hybrid approximation overperforms the others. As for energy purposes, it not only succeeds in accurately describing the density within the covalent bond region, but also provides a good estimate of the density within noncovalent bond areas. In this sense, the double hybrid scheme achieves adding to the electron density the missing nonlocal correlation that a classical dispersion correction brings only to the energy but not to the density.

As a third conclusion, we revealed the absence of linear correlation between energy and density performance for the 20 highly parameterized density functionals selected here. Most of them overperform nonempirical and minimally parameterized approaches of the same category regarding energy properties, however their density performance improvement, even

if it exists and remains of course excellent, is generally not as large as the one found for energy. We particularly showed that the M06-2X global-hybrid approximation is the most accurate in term of density-based and energy properties, and that the ωB97 family of functionals could be also recommended if paying a special attention to the dispersion-corrected variants. In this sense, it is worth to note that highly parameterized density functionals can be also recommended to tackle topological investigations of the density.

Finally, by studying the density-driven error, we emphasized that a good quality density does not guarantee a good energy when dealing with highly parameterized functionals. In this sense, we strongly encourage to use them in a self-consistent fashion. However, in the specific case a non-self-consistent computation would be required, we showed that a density produced by a global hybrid including between 25 and $\sim$50% of EXX is the best compromise to recover the self-consistent performances.

Acknowledgement

E.B. and V.T. gratefully acknowledge GDR 3333 RFCT CNRS for their financial support through the call for proposals "Soutien à des collaborations scientifiques". E.B. thanks ANR (Agence Nationale de la Recherche) and CGI (Commissariat à l'Investissement d'Avenir) for their financial support of this work through Labex SEAM (Science and Engineering for Advanced Materials and devices) ANR-10-LABX-096, ANR-18-IDEX-0001. V.T. and L.J. thank the Labex SynOrg (ANR-11-2ABX-0029) for funding. The authors acknowledge the GENCI-CINES and the CRIANN centers for HPC resources (Projects A0080810359 and A0100810359) just like the local P3MB HPC platform of Université de Paris (ANR-18-IDEX-0001).

Supporting Information Available

Within Supporting Information, Figure S1 depicts the linear relationship between density errors integrated globally on a grid and evaluated locally at critical point. Figures S2 to S9 complement Figures 2, 4 and 5 by providing statistics calculated (*i*) on the larger G2, DBH24 and NCB31 datasets, and (*ii*) in function of the CP type. Tables S1 to S6 report the detailed results of global density overlap functions estimated from the systems gathered the tested databases. A detailed list of all the reaction energies and QTAIM descriptors computed for each molecular systems is reported in Tables S7 to S12 (energy property), Tables S13 to S205 (density property), and Tables S206 to S397 (Laplacian of the density property).

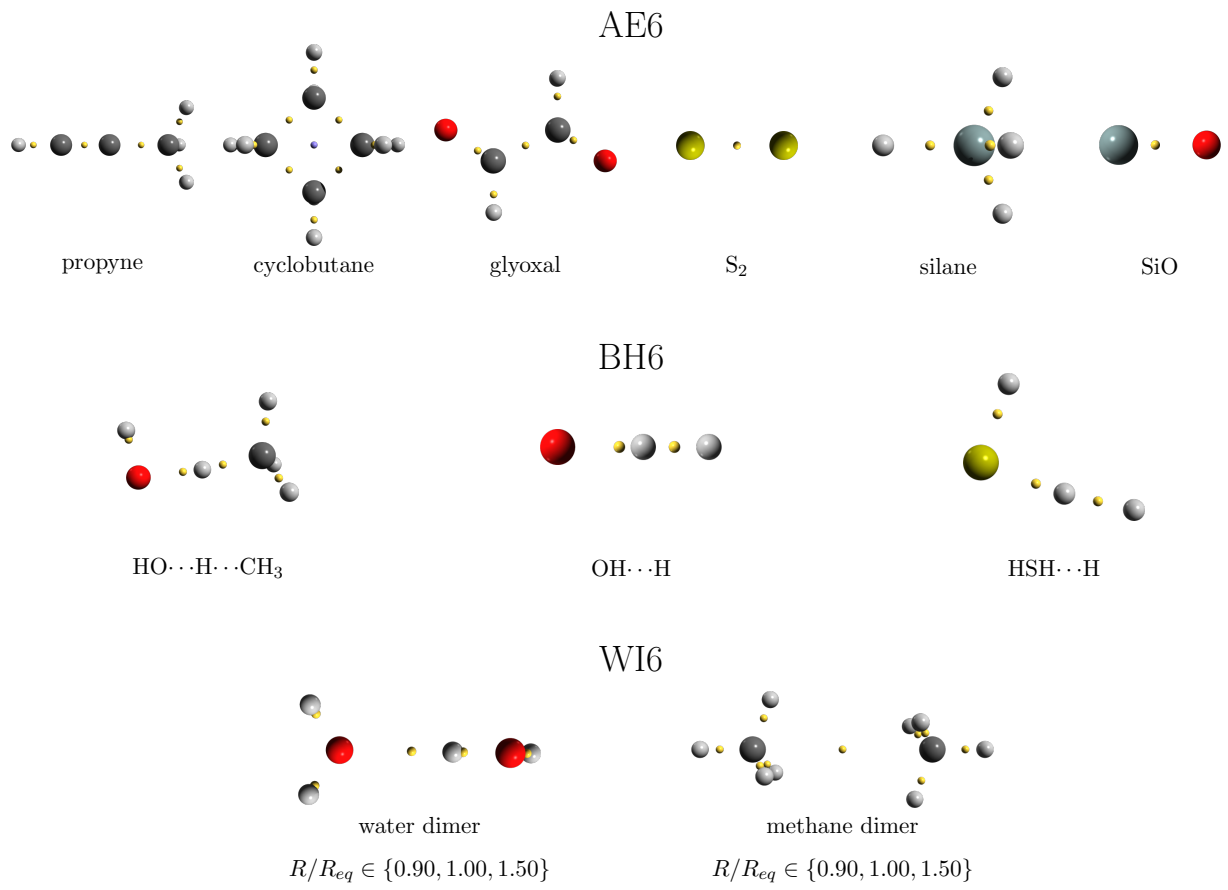

Figure 1: Views of the 15 QTAIM molecular topologies under investigation within the 3 representative databases, computed at the CCSD/def2-QZVP reference level of theory. Six of them (top) derive from the representative AE6 atomization energy database and count a total of 29 $(3,-1)$ bond + 1 $(3,+1)$ ring reference critical points (CPs). Three of them (middle) are the transition-state structures considered in the representative BH6 barrier height energy database and gathers 11 $(3,-1)$ bond reference CPs. The last six (down) are gathered into the WI6 weak-interaction energy database. They probe six reference CPs governing the six weak intermolecular interactions. The entire set of molecules gathers a total of 47 reference CPs. Color code: H in white, C in grey, O in red, S in dark yellow, Si in blue, $(3,-1)$ bond CP in bright yellow, and $(3,+1)$ ring CP in purple.

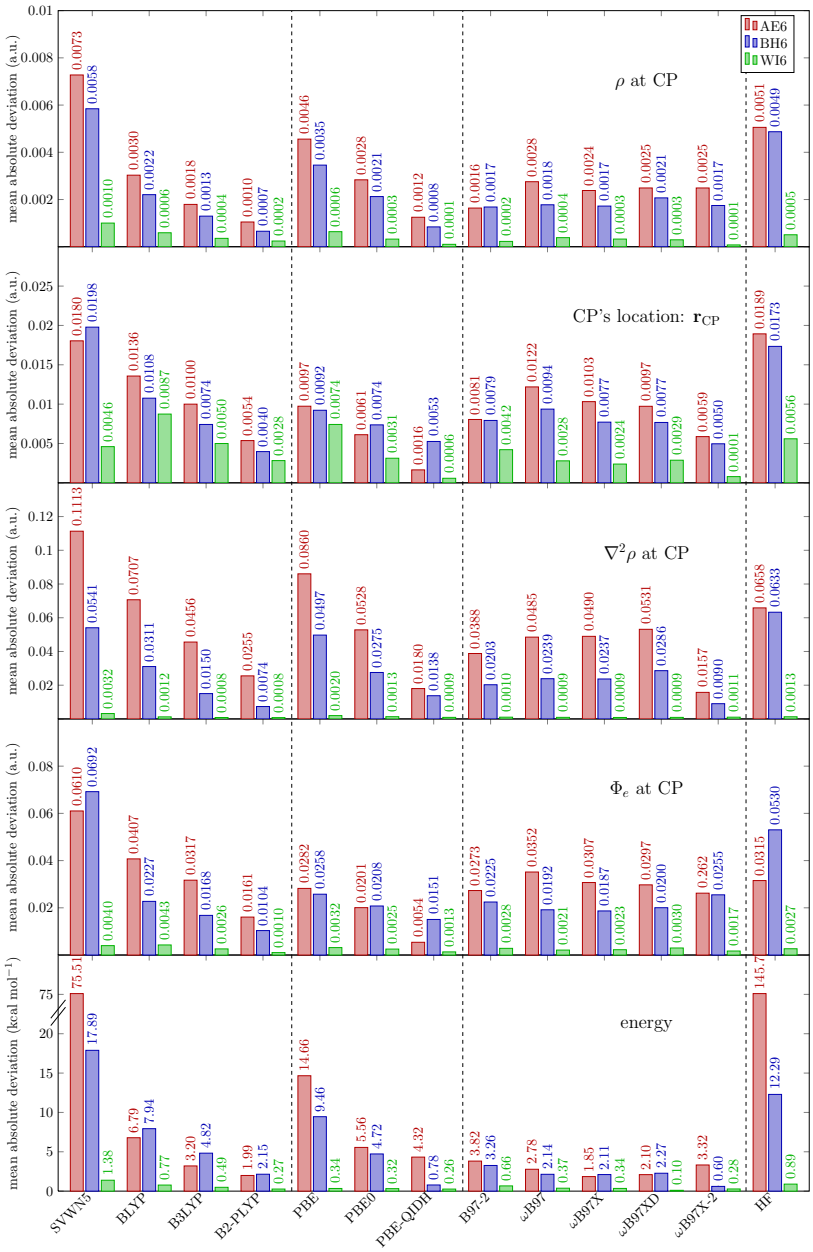

Figure 2: From top to down, mean absolute deviations (MADs) calculated over the density (ρ in a.u.), position ($\mathbf{r}_{\mathrm{CP}}$ in a.u.), Laplacian of the electron density ($\nabla^2\rho$ in a.u.), and electrostatic potential from electrons (Φ_e in a.u.) errors from the 47 critical points gathered into the AE6, BH6 and WI6 representative databases for a selection of density functionals. As a matter of comparison, the energy performance (MADs in kcal mol^{-1}) of each density functional is provided in the down panel. All computations are performed with the def2-QZVP basis set.

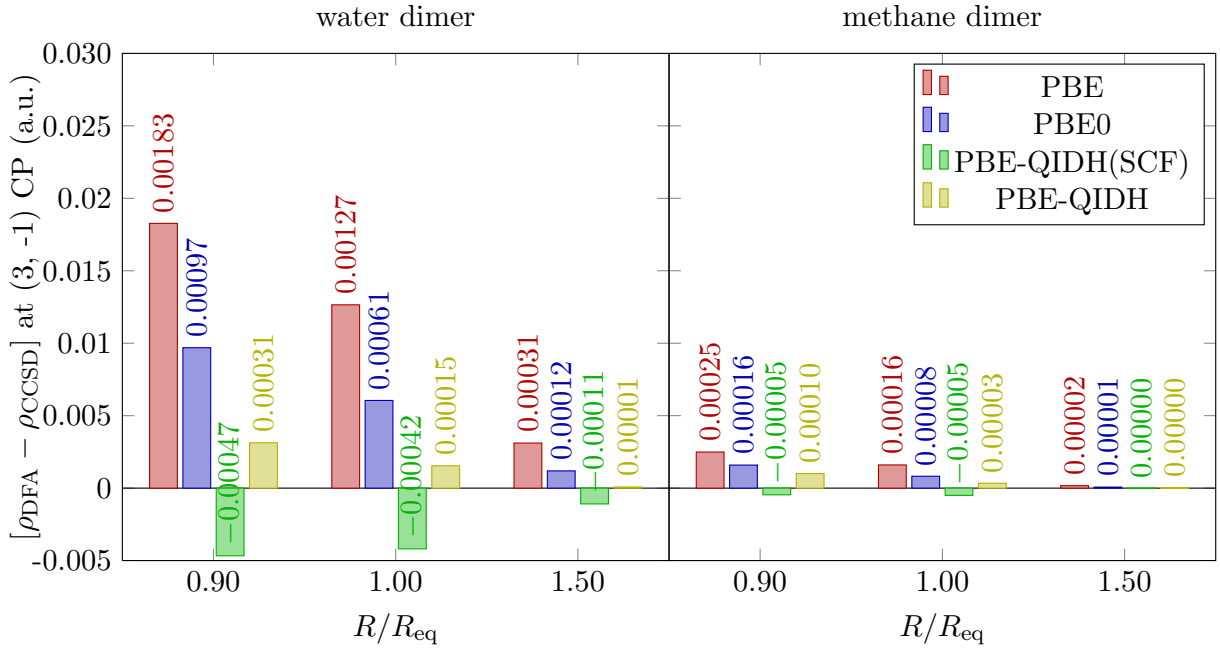

Figure 3: Density difference with the CCSD reference ($[\rho_{\mathrm{DFA}} - \rho_{\mathrm{CCSD}}]$ in a.u.) evaluated at the $(3, -1)$ critical point governing the weak interaction in the water and methane dimer systems at three selected points on their dissociation path (WI6 database) for a selection of density functionals at the def2-QZVP level of theory.

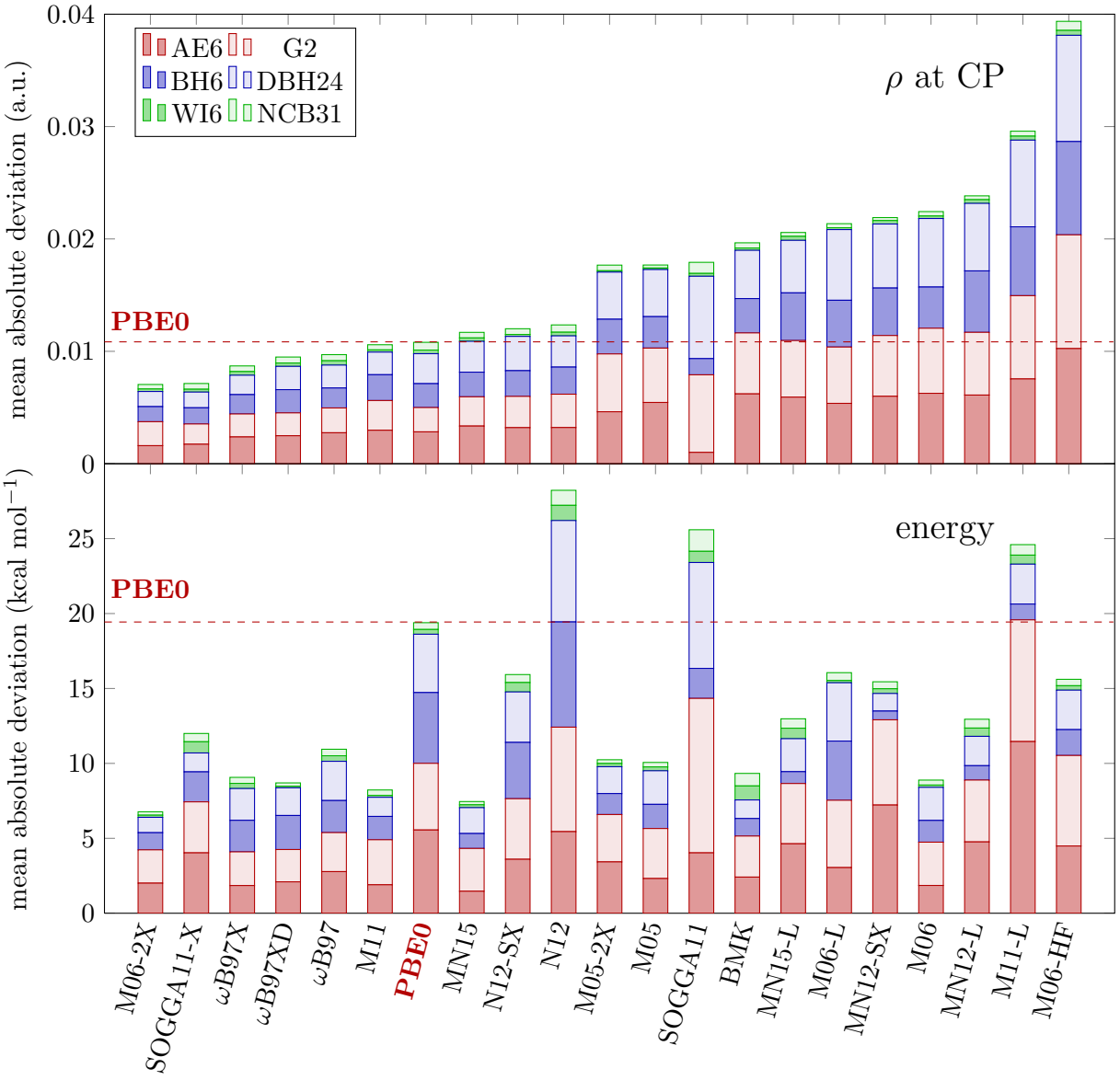

Figure 4: Mean absolute deviations (MADs) calculated over the (top) density (ρ in a.u.) at critical points, and (down) reaction energy (in kcal mol^{-1}) errors on the atomization energy (AE6 and G2 in red and light red, respectively), barrier height (BH6 and DBH24 in blue and light blue, respectively) and weak interaction (WI6 and NCB31 in green and light greeen, respectively) databases for a selection of 20 highly parameterized density functionals (see Section S2 within Supporting Information). The performance of the nonempirical PBE0 density functional regarding these databases is provided as the sake of comparison. All the computations are performed with the def2-QZVP basis set.

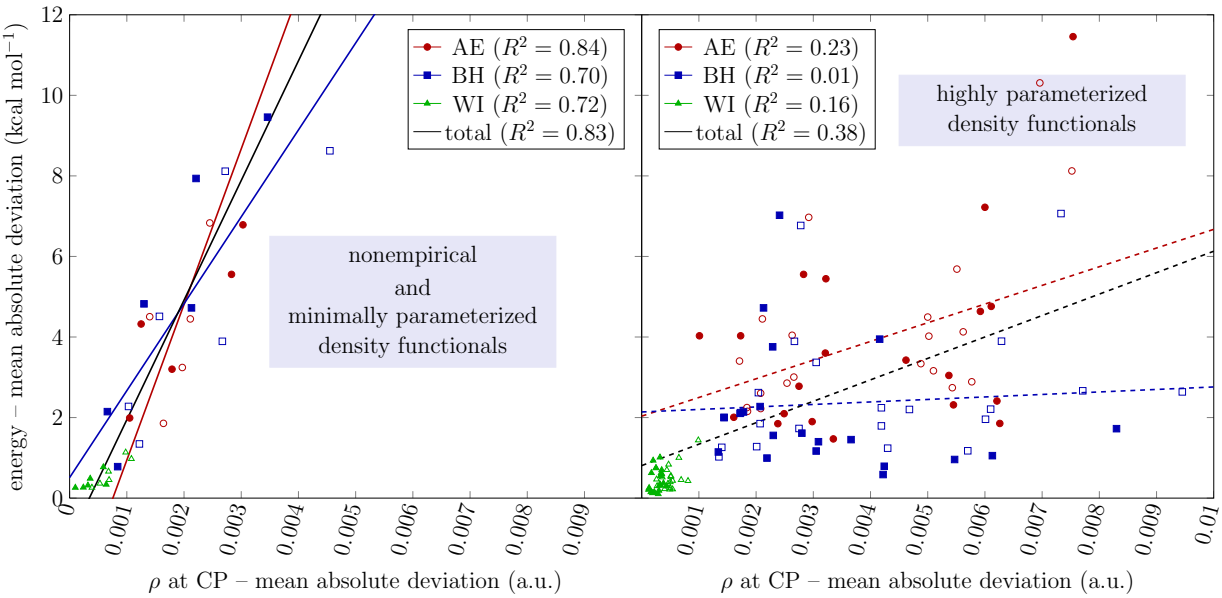

Figure 5: Correlation diagrams between the density and energy mean absolute deviation (MAD) criteria for (left) PBE- and BLYP-based nonempirical and minimally parameterized density functionals, and (right) a selection of 20 highly parameterized density functionals (see Section S2 within Supporting Information) on the (red) atomization energy [AE: AE6 (empty circles) and G2 (filled circles)], (blue) barrier height [BH: BH6 (empty squares) and DBH24 (filled squares), and (green) weak interaction [WI: WI6 (empty triangles) and NCB31 (filled triangles)] databases. For each database and the whole databases (black), the coefficients of determination (R^2) related to each linear regression are provided in the legend. See Figures S3 and S5 within Supporting Information for more detailed statistics on the single datasets.

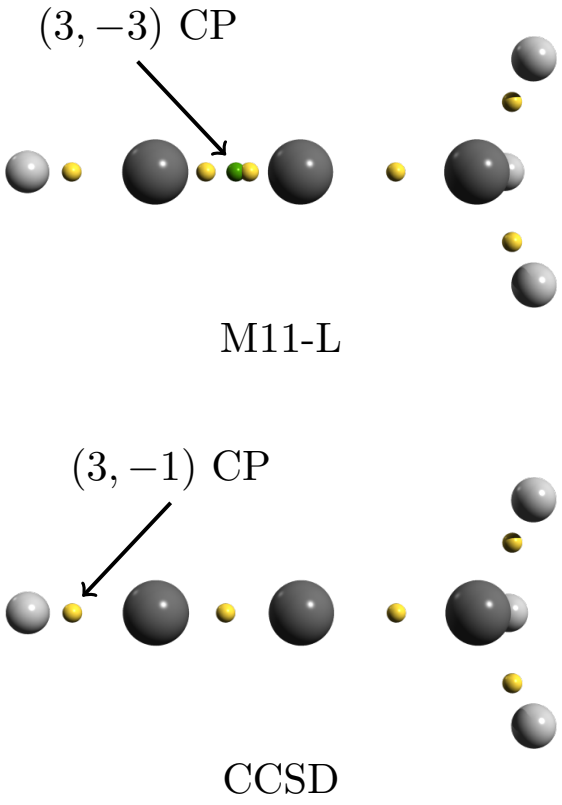

Figure 6: Comparison between the quantum theory of atoms-in-molecules (QTAIM) molecular topology of propyne derived from the M11-L density functional density and the reference CCSD approach. All the computations are performed with the def2-QZVP basis set. Colour code: H in white, C in grey, $(3, -1)$ bond CP in yellow, and $(3, -3)$ non nuclear attractor CP in green.

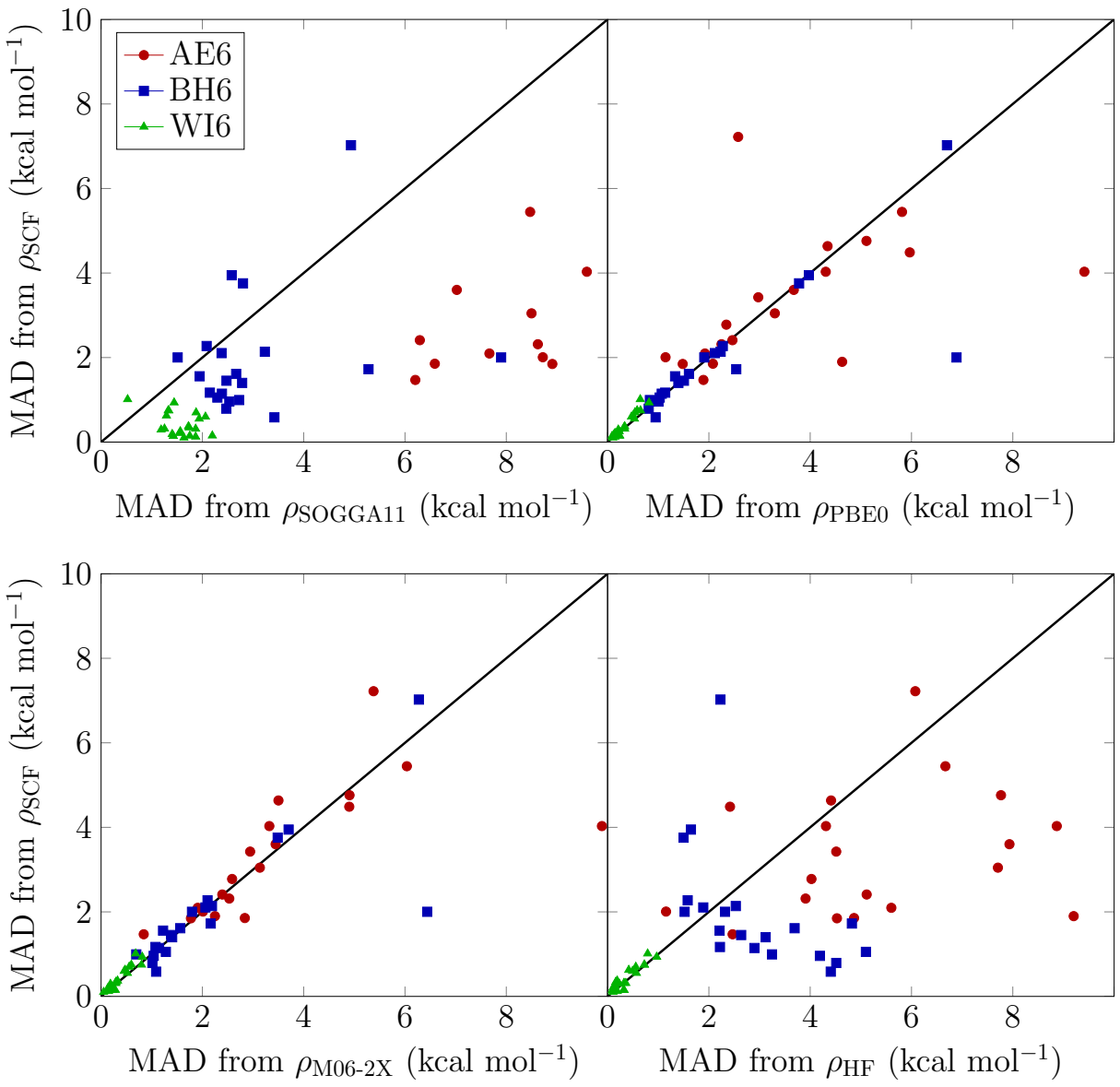

Figure 7: Correlation diagram depicting the energy- versus density-driven errors on the performance (MADs in kcal mol^{-1}) of a selection of 20 highly parameterized density functionals on the (red) AE6, (blue) BH6, and (green) WI6 databases. All the computations are performed with the def2-QZVP basis set. A lower deviation to the diagonal means here a decreasing performance of the non-self-consistent approach.

References

(1) Hohenberg, P.; Kohn, W. Inhomogeneous Electron Gas. *Phys. Rev. B* **1964**, *136*, 864–871.

(2) Peverati, R.; Truhlar, D. G. Quest for a universal density functional: the accuracy of density functionals across a broad spectrum of databases in chemistry and physics. *Phil. Trans. R. Soc. A* **2014**, *372*, 20120476.

(3) Mardirossian, N.; Head-Gordon, M. Thirty years of density functional theory in computational chemistry: an overview and extensive assessment of 200 density functionals. *Mol. Phys.* **2017**, *115*, 2315–2372.

(4) Goerigk, L.; Hansen, A.; Bauer, C.; Ehrlich, S.; Najibi, A.; Grimme, S. A look at the density functional theory zoo with the advanced GMTKN55 database for general main group thermochemistry, kinetics and noncovalent interactions. *Phys. Chem. Chem. Phys.* **2017**, *19*, 32184–32215.

(5) Puzzarini, C.; Barone, V. Diving for Accurate Structures in the Ocean of Molecular Systems with the Help of Spectroscopy and Quantum Chemistry. *Acc. Chem. Res.* **2018**, *51*, 548–556.

(6) Penocchio, E.; Piccardo, M.; Barone, V. Semiexperimental Equilibrium Structures for Building Blocks of Organic and Biological Molecules: The B2PLYP Route. *J. Chem. Theory Comput.* **2015**, *11*, 4689–4707.

(7) Brémond, E.; Savarese, M.; Adamo, C.; Jacquemin, D. Accuracy of TD-DFT Geometries: A Fresh Look. *J. Chem. Theory Comput.* **2018**, *14*, 3715–3727.

(8) Budzák, S.; Scalmani, G.; Jacquemin, D. Accurate Excited-State Geometries: A CASPT2 and Coupled-Cluster Reference Database for Small Molecules. *J. Chem. Theory Comput.* **2017**, *13*, 6237–6252.

(9) Loos, P.-F.; Scemama, A.; Jacquemin, D. The Quest for Highly Accurate Excitation Energies: A Computational Perspective. *J. Phys. Chem. Lett.* **2020**, *11*, 2374–2383.

(10) Loos, P.-F.; Lipparini, F.; Boggio-Pasqua, M.; Scemama, A.; Jacquemin, D. A Mountaineering Strategy to Excited States: Highly Accurate Energies and Benchmarks for Medium Sized Molecules. *J. Chem. Theory Comput.* **2020**, *16*, 1711–1741.

(11) Brémond, E.; Savarese, M.; Pérez-Jiménez, A. J.; Sancho-García, J. C.; Adamo, C. Speed-Up of the Excited-State Benchmarking: Double-Hybrid Density Functionals as Test Cases. *J. Chem. Theory Comput.* **2017**, *13*, 5539–5551.

(12) Leang, S. S.; Zahariev, F.; Gordon, M. S. Benchmarking the performance of time-dependent density functional methods. *J. Chem. Phys.* **2012**, *136*, 104101.

(13) Schreiber, M.; Silva-Junior, M. R.; Sauer, S. P. A.; Thiel, W. Benchmarks for electronically excited states: CASPT2, CC2, CCSD, and CC3. *J. Chem. Phys.* **2008**, *128*, 134110.

(14) Levy, M. Universal variational functionals of electron densities, first-order density matrices, and natural spin-orbitals and solution of the v-representability problem. *Proc. Natl. Acad. Sci. U.S.A.* **1979**, *76*, 6062–6065.

(15) Kohn, W.; Sham, L. J. Self-Consistent Equations Including Exchange and Correlation Effects. *Phys. Rev. A* **1965**, *140*, 1133–1138.

(16) Cruz, F. G.; Lam, K.-C.; Burke, K. Exchange-Correlation Energy Density from Virial Theorem. *J. Phys. Chem. A* **1998**, *102*, 4911–4917.

(17) Solà, M.; Mestres, J.; Carbó, R.; Duran, M. A comparative analysis by means of quantum molecular similarity measures of density distributions derived from conventional ab initio and density functional methods. *J. Chem. Phys.* **1996**, *104*, 636–647.

(18) Worsnop, S. K.; Wang, J.; Boyd, R. J. An orbital-based density difference index for the comparison of electron density distributions. *J. Chem. Phys.* **1997**, *107*, 6693–6698.

(19) Boyd, R. J.; Wang, J.; Eriksson, L. A. *Recent Advances in Density Functional Methods*; Workd Scientific, 1995; pp 369–401.

(20) Carbó, R.; Besalú, E.; Amat, L.; Fradera, X. On quantum molecular similarity measures (QMSM) and indices (QMSI). *J. Math. Chem.* **1996**, *19*, 47–56.

(21) Carbó, R.; Leyda, L.; Arnau, M. How similar is a molecule to another? An electron density measure of similarity between two molecular structures. *Int. J. Quantum Chem.* **1980**, *17*, 1185–1189.

(22) Bultinck, P.; Gironés, X.; Carbó-Dorcaz, R. *Reviews in Computational Chemistry*; John Wiley & Sons, Ltd, 2005; Chapter 2, pp 127–207.

(23) Medvedev, M. G.; Bushmarinov, I. S.; Sun, J.; Perdew, J. P.; Lyssenko, K. A. Density functional theory is straying from the path toward the exact functional. *Science* **2017**, *355*, 49–52.

(24) Korth, M. Density Functional Theory: Not Quite the Right Answer for the Right Reason Yet. *Angew. Chem. Int.* **2017**, *56*, 5396–5398.

(25) Kepp, K. P. Comment on "Density functional theory is straying from the path toward the exact functional". *Science* **2017**, *356*, 496–496.

(26) Wang, Y.; Wang, X.; Truhlar, D. G.; He, X. How Well Can the M06 Suite of Functionals Describe the Electron Densities of Ne, Ne6+, and Ne8+? *J. Chem. Theory Comput.* **2017**, *13*, 6068–6077.

(27) Ranasinghe, D. S.; Perera, A.; Bartlett, R. J. A note on the accuracy of KS-DFT densities. *J. Chem. Phys.* **2017**, *147*, 204103.

(28) Gould, T. What Makes a Density Functional Approximation Good? Insights from the Left Fukui Function. *J. Chem. Theory Comput.* **2017**, *13*, 2373–2377.

(29) Sim, E.; Song, S.; Burke, K. Quantifying Density Errors in DFT. *J. Phys. Chem. Lett.* **2018**, *9*, 6385–6392.

(30) Hammes-Schiffer, S. A conundrum for density functional theory. *Science* **2017**, *355*, 28–29.

(31) Graziano, G. Quantum chemistry: DFT's midlife crisis. *Nat. Rev. Chem.* **2017**, *1*, 2397–3358.

(32) Medvedev, M. G.; Bushmarinov, I. S.; Sun, J.; Perdew, J. P.; Lyssenko, K. A. Response to Comment on "Density functional theory is straying from the path toward the exact functional". *Science* **2017**, *356*, 496–496.

(33) Johnson, E. R.; Becke, A. D.; Sherrill, C. D.; DiLabio, G. A. Oscillations in meta-generalized-gradient approximation potential energy surfaces for dispersion-bound complexes. *J. Chem. Phys.* **2009**, *131*, 034111.

(34) Wheeler, S. E.; Houk, K. N. Integration Grid Errors for Meta-GGA-Predicted Reaction Energies: Origin of Grid Errors for the M06 Suite of Functionals. *J. Chem. Theory Comput.* **2010**, *6*, 395–404.

(35) Brorsen, K. R.; Yang, Y.; Pak, M. V.; Hammes-Schiffer, S. Is the Accuracy of Density Functional Theory for Atomization Energies and Densities in Bonding Regions Correlated? *J. Phys. Chem. Lett.* **2017**, *8*, 2076–2081.

(36) Perdew, J. P.; Ruzsinszky, A.; Constantin, L. A.; Sun, J.; Csonka, G. I. Some Fundamental Issues in Ground-State Density Functional Theory: A Guide for the Perplexed. *J. Chem. Theory Comput.* **2009**, *5*, 902–908.

(37) Mezei, P. D.; Csonka, G. I.; Kállay, M. Electron Density Errors and Density-Driven Exchange-Correlation Energy Errors in Approximate Density Functional Calculations. *J. Chem. Theory Comput.* **2017**, *13*, 4753–4764.

(38) Su, N. Q.; Zhu, Z.; Xu, X. Doubly hybrid density functionals that correctly describe both density and energy for atoms. *Proc. Natl. Acad. Sci. U.S.A.* **2018**, *115*, 2287–2292.

(39) Laplaza, R.; Polo, V.; Contreras-García, J. Localizing electron density errors in density functional theory. *Phys. Chem. Chem. Phys.* **2019**, *21*, 20927–20938.

(40) Brémond, E.; Savarese, M.; Pérez-Jiménez, A. J.; Sancho-García, J. C.; Adamo, C. Systematic Improvement of Density Functionals through Parameter-Free Hybridization Schemes. *J. Phys. Chem. Lett.* **2015**, *6*, 3540–3545.

(41) Bochevarov, A. D.; Friesner, R. A. The densities produced by the density functional theory: Comparison to full configuration interaction. *J. Chem. Phys.* **2008**, *128*, 034102.

(42) Hait, D.; Head-Gordon, M. How Accurate Is Density Functional Theory at Predicting Dipole Moments? An Assessment Using a New Database of 200 Benchmark Values. *J. Chem. Theory Comput.* **2018**, *14*, 1969–1981.

(43) Verma, P.; Truhlar, D. G. Can Kohn–Sham density functional theory predict accurate charge distributions for both single-reference and multi-reference molecules? *Phys. Chem. Chem. Phys.* **2017**, *19*, 12898–12912.

(44) Bader, R. F. W. *Atoms in Molecules: A Quantum Theory*; Oxford University Press: Oxford, U.K., 1990.

(45) Popelier, P. L. A. *Atoms in Molecules: An Introduction*; Pearson Education: Harlow, U.K., 2000.

(46) Becke, A. D.; Edgecombe, K. E. A simple measure of electron localization in atomic and molecular systems. *J. Chem. Phys.* **1990**, *92*, 5397–5403.

(47) Schmider, H.; Becke, A. Chemical content of the kinetic energy density. *J. Mol. Struct.: THEOCHEM* **2000**, *527*, 51–61.

(48) de Silva, P.; Corminboeuf, C. Simultaneous Visualization of Covalent and Noncovalent Interactions Using Regions of Density Overlap. *J. Chem. Theory Comput.* **2014**, *10*, 3745–3756.

(49) Vannay, L.; Brémond, E.; de Silva, P.; Corminboeuf, C. Visualizing and Quantifying Interactions in the Excited State. *Chem. Eur. J.* **2016**, *22*, 18442–18449.

(50) Tognetti, V.; Joubert, L. On the Influence of Density Functional Approximations on Some Local Bader's Atoms-in-Molecules Properties. *J. Phys. Chem. A* **2011**, *115*, 5505–5515.

(51) Rykounov, A. A.; Tsirelson, V. G. Quantitative estimates of transferability of the QTAIM descriptors. Case study of the substituted hydropyrimidines. *J. Mol. Struct.* **2009**, *906*, 11–24.

(52) Yau, A. D.; Byrd, E. F. C.; Rice, B. M. An Investigation of KS-DFT Electron Densities used in Atoms-in-Molecules Studies of Energetic Molecules. *J. Phys. Chem. A* **2009**, *113*, 6166–6171.

(53) Jabłoński, M.; Palusiak, M. Basis Set and Method Dependence in Atoms in Molecules Calculations. *J. Phys. Chem. A* **2010**, *114*, 2240–2244.

(54) Jabłoński, M.; Palusiak, M. Basis Set and Method Dependence in Atoms in Molecules Calculations. *J. Phys. Chem. A* **2010**, *114*, 2240–2244.

(55) Martín Pendás, A.; Blanco, M.; Francisco, E. Revisiting the variational nature of the quantum theory of atoms in molecules. *Chem. Phys. Lett.* **2006**, *417*, 16 – 21.

(56) Bader, R. F. W. Principle of stationary action and the definition of a proper open system. *Phys. Rev. B* **1994**, *49*, 13348–13356.

(57) Bader, R. F. W.; Popelier, P. L. A. Atomic theorems. *Int. J. Quantum Chem.* **1993**, *45*, 189–207.

(58) Mohajeri, A.; Ashrafi, A. Aromaticity in terms of ring critical point properties. *Chem. Phys. Lett.* **2008**, *458*, 378–383.

(59) Emamian, S.; Lu, T.; Kruse, H.; Emamian, H. Exploring Nature and Predicting Strength of Hydrogen Bonds: A Correlation Analysis Between Atoms-in-Molecules Descriptors, Binding Energies, and Energy Components of Symmetry-Adapted Perturbation Theory. *J. Comput. Chem.* **2019**, *40*, 2868–2881.

(60) Shahi, A.; Arunan, E. Hydrogen bonding, halogen bonding and lithium bonding: an atoms in molecules and natural bond orbital perspective towards conservation of total bond order, inter- and intra-molecular bonding. *Phys. Chem. Chem. Phys.* **2014**, *16*, 22935–22952.

(61) Grabowski, S. J. QTAIM Characteristics of Halogen Bond and Related Interactions. *J. Phys. Chem. A* **2012**, *116*, 1838–1845.

(62) Parthasarathi, R.; Subramanian, V.; Sathyamurthy, N. Hydrogen Bonding in Phenol, Water, and Phenol-Water Clusters. *J. Phys. Chem. A* **2005**, *109*, 843–850.

(63) Koch, U.; Popelier, P. L. A. Characterization of C-H-O Hydrogen Bonds on the Basis of the Charge Density. *J. Phys. Chem.* **1995**, *99*, 9747–9754.

(64) Bader, R. F. W.; Essén, H. The characterization of atomic interactions. *J. Chem. Phys.* **1984**, *80*, 1943–1960.

(65) Tognetti, V.; Joubert, L. Density functional theory and Bader's atoms-in-molecules theory: towards a vivid dialogue. *Phys. Chem. Chem. Phys.* **2014**, *16*, 14539–14550.

(66) Tognetti, V.; Joubert, L.; Cortona, P.; Adamo, C. Toward a Combined DFT/QTAIM Description of Agostic Bonds: The Critical Case of a Nb(III) Complex. *J Phys. Chem. A* **2009**, *113*, 12322–12327.

(67) Keith, T. A.; Bader, R. F. W.; Aray, Y. Structural homeomorphism between the electron density and the virial field. *Int. J. Quantum Chem.* **1996**, *57*, 183–198.

(68) Patrikeev, L.; Joubert, L.; Tognetti, V. Atomic decomposition of Kohn-Sham molecular energies: the kinetic energy component. *Mol. Phys.* **2016**, *114*, 1285–1296.

(69) Becke, A. D. A new mixing of Hartree-Fock and local density-functional theories. *J. Chem. Phys.* **1993**, *98*, 1372–1377.

(70) Becke, A. D. Density-functional thermochemistry. III. The role of exact exchange. *J. Chem. Phys.* **1993**, *98*, 5648–5652.

(71) Yanai, T.; Tew, D.; Handy, N. A new hybrid exchange-correlation functional using the Coulomb-attenuating method (CAM-B3LYP). *Chem. Phys. Lett.* **2004**, *393*, 51–57.

(72) Tawada, Y.; Tsuneda, T.; Yanagisawa, S.; Yanai, T.; Hirao, K. A long-range-corrected time-dependent density functional theory. *J. Chem. Phys.* **2004**, *120*, 8425–8433.

(73) Iikura, H.; Tsuneda, T.; Yanai, T.; Hirao, K. A long-range correction scheme for generalized-gradient-approximation exchange functionals. *J. Chem. Phys.* **2001**, *115*, 3540–3544.

(74) Brémond, E.; Ciofini, I.; Sancho-García, J. C.; Adamo, C. Nonempirical Double-Hybrid Functionals: An Effective Tool for Chemists. *Acc. Chem. Res.* **2016**, *49*, 1503–1513.

(75) Goerigk, L.; Grimme, S. Double-hybrid density functionals. *WIREs Comput. Mol. Sci.* **2014**, *4*, 576–600.

(76) Sancho-García, J. C.; Adamo, C. Double-hybrid density functionals: merging wave-function and density approaches to get the best of both worlds. *Phys. Chem. Chem. Phys.* **2013**, *15*, 14581–14594.

(77) Bao, J. L.; Gagliardi, L.; Truhlar, D. G. Self-Interaction Error in Density Functional Theory: An Appraisal. *J. Phys. Chem. Lett.* **2018**, *9*, 2353–2358.

(78) Cohen, A. J.; Mori-Sánchez, P.; Yang, W. Insights into Current Limitations of Density Functional Theory. *Science* **2008**, *321*, 792–794.

(79) Harris, J. Adiabatic-connection approach to Kohn-Sham theory. *Phys. Rev. A* **1984**, *29*, 1648–1659.

(80) Frisch, M. J.; Trucks, G. W.; Schlegel, H. B.; Scuseria, G. E.; Robb, M. A.; Cheeseman, J. R.; Scalmani, G.; Barone, V.; Petersson, G. A.; Nakatsuji, H.; Li, X.; Caricato, M.; Marenich, A. V.; Bloino, J.; Janesko, B. G.; Gomperts, R.; Mennucci, B.; Hratchian, H. P.; Ortiz, J. V.; Izmaylov, A. F.; Sonnenberg, J. L.; Williams-Young, D.; Ding, F.; Lipparini, F.; Egidi, F.; Goings, J.; Peng, B.; Petrone, A.; Henderson, T.; Ranasinghe, D.; Zakrzewski, V. G.; Gao, J.; Rega, N.; Zheng, G.; Liang, W.; Hada, M.; Ehara, M.; Toyota, K.; Fukuda, R.; Hasegawa, J.; Ishida, M.; Nakajima, T.; Honda, Y.; Kitao, O.; Nakai, H.; Vreven, T.; Throssell, K.; Montgomery, J. A., Jr.; Peralta, J. E.; Ogliaro, F.; Bearpark, M. J.; Heyd, J. J.; Brothers, E. N.; Kudin, K. N.; Staroverov, V. N.; Keith, T. A.; Kobayashi, R.; Normand, J.; Raghavachari, K.; Rendell, A. P.; Burant, J. C.; Iyengar, S. S.; Tomasi, J.; Cossi, M.; Millam, J. M.; Klene, M.; Adamo, C.; Cammi, R.; Ochterski, J. W.; Martin, R. L.; Morokuma, K.; Farkas, O.; Foresman, J. B.; Fox, D. J. Gaussian˜16 Revision C.01. 2016; Gaussian Inc. Wallingford CT.

(81) Weigend, F.; Ahlrichs, R. Balanced basis sets of split valence, triple zeta valence and

quadruple zeta valence quality for H to Rn: Design and assessment of accuracy. *Phys. Chem. Chem. Phys.* **2005**, *7*, 3297–3305.

(82) Neese, F.; Wennmohs, F.; Becker, U.; Riplinger, C. The ORCA quantum chemistry program package. *J. Chem. Phys.* **2020**, *152*, 224108.

(83) Neese, F.; Wennmohs, F.; Hansen, A.; Becker, U. Efficient, approximate and parallel Hartree-Fock and hybrid DFT calculations. A 'chain-of-spheres' algorithm for the Hartree-Fock exchange. *Chem. Phys.* **2009**, *356*, 98–109.

(84) Wiberg, K. B.; Hadad, C. M.; LePage, T. J.; Breneman, C. M.; Frisch, M. J. Analysis of the effect of electron correlation on charge density distributions. *J. Phys. Chem.* **1992**, *96*, 671–679.

(85) Handy, N. C.; Schaefer, H. F. On the evaluation of analytic energy derivatives for correlated wave functions. *J. Chem. Phys.* **1984**, *81*, 5031–5033.

(86) Song, S.; Vuckovic, S.; Sim, E.; Burke, K. Density Sensitivity of Empirical Functionals. *J. Phys. Chem. Lett.* **2021**, *12*, 800–807.

(87) Vuckovic, S.; Song, S.; Kozlowski, J.; Sim, E.; Burke, K. Density Functional Analysis: The Theory of Density-Corrected DFT. *J. Chem. Theory Comput.* **2019**, *15*, 6636–6646.

(88) Kim, M.-C.; Sim, E.; Burke, K. Understanding and Reducing Errors in Density Functional Calculations. *Phys. Rev. Lett.* **2013**, *111*, 073003.

(89) Verstraelen, T.; Tecmer, P.; Heidar-Zadeh, F.; González-Espinoza, C. E.; Chan, M.; Kim, T. D.; Boguslawski, K.; Fias, S.; Vandenbrande, S.; Berrocal, D.; Ayers, P. W. HORTON 2.1.1. 2019; `http://theochem.github.com/horton`.

(90) Becke, A. D. A multicenter numerical integration scheme for polyatomic molecules. *J. Chem. Phys.* **1988**, *88*, 2547–2553.

(91) Keith, T. A. AIMAll (Version 19.02.13). 2019; TK Gristmill Software, Overland Park KS, USA, (aim.tkgristmill.com).

(92) Grimme, S. Theoretical Bond and Strain Energies of Molecules Derived from Properties of the Charge Density at Bond Critical Points. *J. Am. Chem. Soc.* **1996**, *118*, 1529–1534.

(93) Cioslowski, J.; Liu, G.; Piskorz, P. Computationally Inexpensive Theoretical Thermochemistry. *J. Phys. Chem. A* **1998**, *102*, 9890–9900.

(94) Lynch, B. J.; Truhlar, D. G. Small Representative Benchmarks for Thermochemical Calculations. *J. Phys. Chem. A* **2003**, *107*, 8996–8999.

(95) Gráfová, L.; Pitoňák, M.; Řezáč, J.; Hobza, P. Comparative Study of Selected Wave Function and Density Functional Methods for Noncovalent Interaction Energy Calculations Using the Extended S22 Data Set. *J. Chem. Theory Comput.* **2010**, *6*, 2365–2376.

(96) Řezáč, J.; Riley, K. E.; Hobza, P. S66: A Well-balanced Database of Benchmark Interaction Energies Relevant to Biomolecular Structures. *J. Chem. Theory Comput.* **2011**, *7*, 2427–2438.

(97) Brauer, B.; Kesharwani, M. K.; Kozuch, S.; Martin, J. M. L. The S66x8 benchmark for noncovalent interactions revisited: explicitly correlated ab initio methods and density functional theory. *Phys. Chem. Chem. Phys.* **2016**, *18*, 20905–20925.

(98) Tognetti, V.; Yahia-Ouahmed, M.; Joubert, L. Comment on "Analysis of CF···FC Interactions on Cyclohexane and Naphthalene Frameworks". *J. Phys. Chem. A* **2014**, *118*, 9791–9792.

(99) Hati, S.; Datta, D. Electronegativity and Bader's bond critical point. *J. Comput. Chem.* **1992**, *13*, 912–918.

(100) Boyd, R. J.; Edgecombe, K. E. Bond critical points in the electronic structures of the main group diatomic hydrides of lithium through bromine. *J. Comput. Chem.* **1987**, *8*, 489–498.

(101) Bousquet, D.; Brémond, E.; Sancho-García, J. C.; Ciofini, I.; Adamo, C. Is There Still Room for Parameter Free Double Hybrids? Performances of PBE0-DH and B2PLYP over Extended Benchmark Sets. *J. Chem. Theory Comput.* **2013**, *9*, 3444–3452.

(102) Mehta, N.; Casanova-Páez, M.; Goerigk, L. Semi-empirical or non-empirical double-hybrid density functionals: which are more robust? *Phys. Chem. Chem. Phys.* **2018**, *20*, 23175–23194.

(103) Berland, K.; Cooper, V. R.; Lee, K.; Schröder, E.; Thonhauser, T.; Hyldgaard, P.; Lundqvist, B. I. van der Waals forces in density functional theory: a review of the vdW-DF method. *Rep. Prog. Phys.* **2015**, *78*, 066501.

(104) Grimme, S.; Hansen, A.; Brandenburg, J. G.; Bannwarth, C. Dispersion-Corrected Mean-Field Electronic Structure Methods. *Chem. Rev.* **2016**, *116*, 5105–5154.

(105) Kong, J.; Gan, Z.; Proynov, E.; Freindorf, M.; Furlani, T. R. Efficient computation of the dispersion interaction with density-functional theory. *Phys. Rev. A* **2009**, *79*, 042510.

(106) Tkatchenko, A.; DiStasio, R. A.; Car, R.; Scheffler, M. Accurate and Efficient Method for Many-Body van der Waals Interactions. *Phys. Rev. Lett.* **2012**, *108*, 236402.

(107) Ikabata, Y.; Sato, T.; Nakai, H. Self-consistent field treatment and analytical energy gradient of local response dispersion method. *I. J. Quantum Chem.* **2013**, *113*, 257–262.

(108) Brémond, E.; Golubev, N.; Steinmann, S. N.; Corminboeuf, C. How important is self-

consistency for the dDsC density dependent dispersion correction? *J. Chem. Phys.* **2014**, *140*, 18A516.

(109) Pople, J. A.; Head-Gordon, M.; Fox, D. J.; Raghavachari, K.; Curtiss, L. A. Gaussian-1 theory: A general procedure for prediction of molecular energies. *J. Chem. Phys.* **1989**, *90*, 5622–5629.

(110) Curtiss, L. A.; Raghavachari, K.; Trucks, G. W.; Pople, J. A. Gaussian-2 theory for molecular energies of first- and second-row compounds. *J. Chem. Phys.* **1991**, *94*, 7221–7230.

(111) Curtiss, L. A.; Raghavachari, K.; Redfern, P. C.; Pople, J. A. Assessment of Gaussian-2 and density functional theories for the computation of enthalpies of formation. *J. Chem. Phys.* **1997**, *106*, 1063–1079.

(112) Zheng, J.; Zhao, Y.; Truhlar, D. G. The DBH24/08 Database and Its Use to Assess Electronic Structure Model Chemistries for Chemical Reaction Barrier Heights. *J. Chem. Theory Comput.* **2009**, *5*, 808–821.

(113) Zhao, Y.; Schultz, N. E.; Truhlar, D. G. Design of Density Functionals by Combining the Method of Constraint Satisfaction with Parametrization for Thermochemistry, Thermochemical Kinetics, and Noncovalent Interactions. *J. Chem. Theory Comput.* **2006**, *2*, 364–382.

(114) Azizi, A.; Momen, R.; Xu, T.; Kirk, S. R.; Jenkins, S. Non-nuclear attractors in small charged lithium clusters, Limq (m = 2–5, q = ±1), with QTAIM and the Ehrenfest force partitioning. *Phys. Chem. Chem. Phys.* **2018**, *20*, 24695–24707.

(115) Terrabuio, L. A.; Teodoro, T. Q.; Matta, C. F.; Haiduke, R. L. A. Nonnuclear Attractors in Heteronuclear Diatomic Systems. *J. Phys. Chem. A* **2016**, *120*, 1168–1174.

(116) Alcoba, D. R.; Lain, L.; Torre, A.; Bochicchio, R. C. Treatments of non-nuclear attractors within the theory of atoms in molecules. *Chem. Phys. Lett.* **2005**, *407*, 379–383.

(117) Cao, W.; Gatti, C.; MacDougall, P.; Bader, R. On the presence of non-nuclear attractors in the charge distributions of Li and Na clusters. *Chem. Phys. Lett.* **1987**, *141*, 380–385.

(118) Santra, G.; Martin, J. M. What Types of Chemical Problems Benefit from Density-Corrected DFT? A Probe Using an Extensive and Chemically Diverse Test Suite. *J. Chem. Theory Comput.* **2021**, *17*, 1368–1379.

(119) Zhang, I. Y.; Su, N. Q.; Brémond, E.; Adamo, C.; Xu, X. Doubly hybrid density functional xDH-PBE0 from a parameter-free global hybrid model PBE0. *J. Chem. Phys.* **2012**, *136*, 174103.

(120) Zhang, I. Y.; Su, N. Q.; Brémond, E.; Adamo, C.; Xu, X. Response to "Comment on 'Doubly hybrid density functional xDH-PBE0 from a parameter-free global hybrid model PBE0"' [J. Chem. Phys. 143, 187101 (2015)]. *J. Chem. Phys.* **2015**, *143*, 187102.

(121) Su, N. Q.; Xu, X. The XYG3 type of doubly hybrid density functionals. *WIREs Comput. Mol. Sci.* **2016**, *6*, 721–747.

(122) Zhang, I. Y.; Xu, X. On the top rung of Jacob's ladder of density functional theory: Toward resolving the dilemma of SIE and NCE. *WIREs Comput. Mol. Sci.* **2021**, *11*, e1490.

(123) Brémond, E.; Savarese, M.; Su, N. Q.; Pérez-Jiménez, A. J.; Xu, X.; Sancho-García, J. C.; Adamo, C. Benchmarking Density Functionals on Structural Parameters of Small-/Medium-Sized Organic Molecules. *J. Chem. Theory Comput.* **2016**, *12*, 459–465.

(124) Slater, J. C. *The Self-Consistent Field for Molecular and Solids, Quantum Theory of Molecular and Solids*; McGraw-Hill: New York, 1974; Vol. 4.

(125) Vosko, S. H.; Wilk, L.; Nusair, M. Accurate spin-dependent electron liquid correlation energies for local spin density calculations: A critical analysis. *Can. J. Phys.* **1980**, *58*, 1200–1211.

(126) Barone, V.; Orlandini, L.; Adamo, C. Proton transfer in model hydrogen-bonded systems by a density functional approach. *Chem. Phys. Lett.* **1994**, *231*, 295–300.

(127) Stephens, P. J.; Devlin, F. J.; Frisch, M. J.; Chabalowski, C. F. Ab initio Calculation of Vibrational Absorption and Circular Dichroism Spectra Using Density Functional Force Fields. *J. Phys. Chem.* **1994**, *98*, 11623–11627.

(128) Chai, J.-D.; Head-Gordon, M. Systematic optimization of long-range corrected hybrid density functionals. *J. Chem. Phys.* **2008**, *128*, 084106.

(129) Grimme, S. Semiempirical hybrid density functional with perturbative second-order correlation. *J. Chem. Phys.* **2006**, *124*, 034108.

(130) Becke, A. D. Density-functional exchange-energy approximation with correct asymptotic-behavior. *Phys. Rev. A* **1988**, *38*, 3098–3100.

(131) Lee, C.; Yang, W.; Parr, R. G. Development of the Colle-Salvetti correlation-energy formula into a functional of the electron density. *Phys. Rev. B* **37**, *1988*, 785–789.

(132) Miehlich, B.; Savin, A.; Stoll, H.; Preuss, H. Results obtained with the correlation-energy density functionals of Becke and Lee, Yang and Parr. *Chem. Phys. Lett.* **1989**, *157*, 200–206.

(133) Wilson, P. J.; Bradley, T. J.; Tozer, D. J. Hybrid exchange-correlation functional determined from thermochemical data and ab initio potentials. *J. Chem. Phys.* **2001**, *115*, 9233–9242.

(134) Brémond, E.; Sancho-García, J. C.; Pérez-Jiménez, A. J.; Adamo, C. Double-hybrid functionals from adiabatic-connection: The QIDH model. *J. Chem. Phys.* **2014**, *141*, 031101–031104.

(135) Perdew, J. P.; Burke, K.; Ernzerhof, M. Generalized gradient approximation made simple. *Phys. Rev. Lett.* **1996**, *77*, 3865–3868.

(136) Adamo, C.; Barone, V. Toward reliable density functional methods without adjustable parameters: The PBE0 model. *J. Chem. Phys.* **1999**, *110*, 6158–6170.

(137) Ernzerhof, M.; Scuseria, G. E. Assessment of the Perdew-Burke-Ernzerhof exchange-correlation functional. *J. Chem. Phys.* **1999**, *110*, 5029–5036.

(138) Chai, J.-D.; Head-Gordon, M. Long-range corrected hybrid density functionals with damped atom-atom dispersion corrections. *Phys. Chem. Chem. Phys.* **2008**, *10*, 6615–6620.

(139) Chai, J.-D.; Head-Gordon, M. Long-range corrected double-hybrid density functionals. *J. Chem. Phys.* **2009**, *131*, 174105.

(140) Peverati, R.; Zhao, Y.; Truhlar, D. G. Generalized Gradient Approximation That Recovers the Second-Order Density-Gradient Expansion with Optimized Across-the-Board Performance. *J. Phys. Chem. Lett.* **2011**, *2*, 1991–1997.

(141) Zhao, Y.; Schultz, N. E.; Truhlar, D. G. Exchange-correlation functional with broad accuracy for metallic and nonmetallic compounds, kinetics, and noncovalent interactions. *J. Chem. Phys.* **2005**, *123*, 161103.

(142) Peverati, R.; Truhlar, D. G. Screened-exchange density functionals with broad accuracy for chemistry and solidstate physics. *Phys. Chem. Chem. Phys.* **2012**, *14*, 16187.

(143) Peverati, R.; Truhlar, D. G. Exchange-Correlation Functional with Good Accuracy for

Both Structural and Energetic Properties while Depending Only on the Density and Its Gradient. *J. Chem. Theory Comput.* **2012**, *8*, 2310–2319.

(144) Zhao, Y.; Schultz, N. E.; Truhlar, D. G. The M06 suite of density functionals for main group thermochemistry, thermochemical kinetics, noncovalent interactions, excited states, and transition elements: two new functionals and systematic testing of four M06-class functionals and 12 other functionals. *Theor. Chem. Acc.* **2008**, *120*, 215–241.

(145) Zhao, Y.; Truhlar, D. G. A new local density functional for main-group thermochemistry, transition metal bonding, thermochemical kinetics, and noncovalent interactions. *J. Chem. Phys.* **2006**, *125*, 194101.

(146) Peverati, R.; Truhlar, D. G. A global hybrid generalized gradient approximation to the exchange-correlation functional that satisfies the second-order density-gradient constraint and has broad applicability in chemistry. *J. Chem. Phys.* **2011**, *135*, 191102.

(147) Peverati, R.; Truhlar, D. G. Improving the Accuracy of Hybrid Meta-GGA Density Functionals by Range Separation. *J. Phys. Chem. Lett.* **2011**, *2*, 2810–2817.

(148) Peverati, R.; Truhlar, D. G. M11-L: A Local Density Functional That Provides Improved Accuracy for Electronic Structure Calculations in Chemistry and Physics. *J. Phys. Chem. Lett.* **2012**, *3*, 117–124.

(149) Boese, A. D.; Martin, J. M. L. Development of Density Functionals for Thermochemical Kinetics. *J. Chem. Phys.* **2004**, *121*, 3405–3416.

(150) Peverati, R.; Truhlar, D. G. An improved and broadly accurate local approximation to the exchange-correlation density functional: The MN12-L functional for electronic structure calculations in chemistry and physics. *Phys. Chem. Chem. Phys.* **2012**, *10*, 13171.

(151) Yu, H. S.; He, X.; Li, S. L.; Truhlar, D. G. MN15: A Kohn–Sham global-hybrid exchange-correlation density functional with broad accuracy for multi-reference and single-reference systems and noncovalent interactions. *Chem. Sci.* **2016**, *7*, 5032–5051.

(152) Yu, H. S.; He, X.; Truhlar, D. G. MN15-L: A New Local Exchange-Correlation Functional for Kohn–Sham Density Functional Theory with Broad Accuracy for Atoms, Molecules, and Solids. *J. Chem. Theory Comput.* **2016**, *12*, 1280–1293.

(153) Zhao, Y.; Schultz, N. E.; Truhlar, D. G. Design of density functionals by combining the method of constraint satisfaction with parametrization for thermochemistry, thermochemical kinetics, and noncovalent interactions. *J. Chem. Theory Comput.* **2006**, *2*, 364–382.

(154) Zhao, Y.; Truhlar, D. G. Comparative DFT study of van der Waals complexes: Rare-gas dimers, alkaline-earth dimers, zinc dimer, and zinc-rare-gas dimers. *J. Phys. Chem.* **2006**, *110*, 5121–5129.

(155) Zhao, Y.; Truhlar, D. G. Density Functional for Spectroscopy: No Long-Range Self-Interaction Error, Good Performance for Rydberg and Charge-Transfer States, and Better Performance on Average than B3LYP for Ground States. *J. Phys. Chem. A* **2006**, *110*, 13126–13130.

Graphical TOC Entry

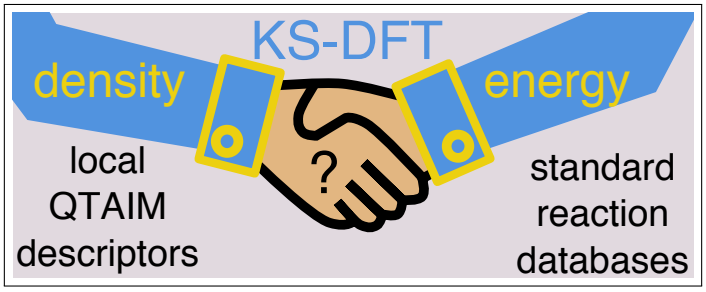

Table 1: List of the exchange-correlation density functionals considered herein. All of them are ordered according to their class of approximation, and their percentages of exact-like exchange (EXX) and correlation computed by second-order perturbation theory (PT2).

non hybrid		global hybrid			range-separated hybrid			double hybrid			
name	Ref.	name	EXX (%)	Ref.	name	EXX (%)	Ref.	name	EXX (%)	PT2 (%)	Ref.
SVWN5	1,15,124,125	B3LYP	20	70,126,127	ωB97	0–100	128	B2-PLYP	53	27	129
BLYP	130–132	B97-2	21	133	ωB97X	16–100	128	PBE-QIDH	69	33	134
PBE	135	PBE0	25	136,137	ωB97X-D	22–100	138	ωB97X-2	68–100	(48,58)[2]	139
SOGGA11	140	M05[1]	27	141	N12-SX	25–0	142				
N12	143	M06[1]	27	144	MN12-SX[1]	25–0	142				
M06-L[1]	145	SOGGA11-X	40	146	M11[1]	43–100	147				
M11-L[1]	148	BMK	42	149							
MN12-L[1]	150	MN15[1]	44	151							
MN15-L[1]	152	M05-2X[1]	56	153							
		M06-2X[1]	54	144							
		M06-HF[1]	100	154,155							

[a] depends on the kinetic energy density (τ).

[b] $(xx,yy) = (c_{os},c_{ss})$ are the opposite- and same-spin component mixing, respectively.